

Backreacted Coulomb energy in the Skyrme model

Sven Bjarke Gudnason¹, James Martin Speight²

¹*Institute of Contemporary Mathematics, School of Mathematics and Statistics, Henan University, Kaifeng, Henan 475004, P. R. China*

²*School of Mathematics, University of Leeds, Leeds LS2 9JT, England*

E-mail: [gudnason\(at\)henu.edu.cn](mailto:gudnason(at)henu.edu.cn), [j.m.speight\(at\)leeds.ac.uk](mailto:j.m.speight(at)leeds.ac.uk)

ABSTRACT: The Skyrme model is extended with the Maxwell action and a source term for the gauge field. We consider the specialized case of vanishing isospin states, such that only an electric potential is turned on and study the backreaction onto the Skyrme fields. In particular, we study Skyrmions with baryon numbers $B = 4, 8, 12, 16$ and 40. We find, in agreement with physical expectations, that the Coulomb backreaction is most pronounced for large Skyrmions and find furthermore that the dynamics of the theory is more sensitive to the backreaction than the ground states (global minimizers of the energy). Calibrating the model to Carbon-12, we find excellent agreement of the masses of the studied Skyrmions – within 1.86% of experimental data. The Coulomb energies are slightly larger than phenomenological fits suggest, but only by about 3 – 22%, whereas the radii are within 15% errors, with the largest errors on the smallest baryon number ($B = 4$) and the smallest errors on the large baryon numbers.

Contents

1	Introduction	1
2	The Skyrme model with Coulomb energy	5
2.1	The field theory	5
2.2	Geometric approach to the variational problem	9
2.3	Derrick scaling	13
2.4	Topological energy bound	14
2.5	Numerical algorithm	14
2.6	Calibration	15
2.7	Skyrmion solutions	21
2.8	The Coulomb energy and the effect of its backreaction	33
3	Conclusion and discussion	40
A	Proof of Lemma 1	43
B	The remaining $B = 40$ solutions	44

1 Introduction

Symmetries are fundamentally important in formulating physical theories of any system. In the strong sector, it so happens that the two lightest quarks are close enough to being massless (compared with the energy scale of the strong interactions) that $SU(2)$ flavour symmetry is a good approximate symmetry. In fact, it is a good approximate symmetry for quarks both with left-handed chirality and right-handed chirality, separately. This fact is called chiral symmetry and the group is $SU(2)_L \times SU(2)_R$. More precisely, the flavour symmetry is classically $U(2)_L \times U(2)_R$ but due to the ABJ anomaly $U(1)_{L-R}$ is anomalous, so the anomaly free symmetry is $SU(2)_L \times SU(2)_R \times U(1)_V$, where the Abelian vector symmetry $V = L + R$ corresponds to the baryon current. Chiral symmetry is broken at, perhaps, the same scale that physics of the strong interactions confines the quarks and all other colour degrees of freedom (the charge or free indices of quarks and gluons). Pions composed by the two lightest quarks, up and down, would be exactly massless if chiral symmetry were an exact symmetry of Nature. Chiral symmetry breaking, nevertheless, is a small effect, leaving the pions as the lightest particles of the strong sector.

The pions can be neatly arranged in a matrix form

$$U = e^{i\pi^a \tau^a F_\pi^{-1}}, \quad U \rightarrow V_L U V_R^\dagger, \quad V_L \in \text{SU}(2)_L, \quad V_R \in \text{SU}(2)_R, \quad (1.1)$$

with F_π called the pion decay constant, π^a the three pions, τ^a the three Pauli matrices, V_L the left flavour transformation matrices and V_R the right flavour transformation matrices. The left- and right-invariant chiral currents, $L_\mu = U^\dagger \partial_\mu U$ and $R_\mu = \partial_\mu U U^\dagger$ are the building blocks of the mesonic sector of chiral perturbation theory (ChPT) [1]. The pure pion operators in ChPT up to p^4 (i.e. a common notation for operators including no more than 4 derivatives) consist of 3 terms, with the lowest-order term being simply the kinetic term for the pions. A particular combination of the two fourth-order derivative terms, that has no more than 2 time derivatives, is called the Skyrme term and is the foundation of the Skyrme model [2, 3]. The Skyrme term is crucial for the simplest model, as it allows for simple Hamiltonian quantization of zero modes and it prevents the soliton of the theory – the Skyrmion – from collapsing.

It is important to notice that the flavour symmetries until now are global symmetries. That is, they are not gauged. What are gauged symmetries then? They are related to and responsible for all known fundamental forces (with the exception of gravity, where it is not known how or if a quantum mechanical fundamental theory lies behind the “classical” gravitational attractive force)¹. The three well-tested fundamental forces in the standard model correspond to U(1), SU(2) and SU(3) gauge groups, which represent electromagnetism, the weak nuclear force and strong nuclear force, respectively.

One could naively think that gauging the U(1)_V part of the chiral symmetry would correspond to including electromagnetism in the model. If the generator is simply the unit matrix, this gives all the components and hence all the “quarks” the same charge, which is known from phenomenology to be wrong. Indeed gauging U(1)_V would correspond to gauging the baryon symmetry, which has been considered in some Beyond-Standard-Model (BSM) physics [5]. The fact that the quarks have different electric charges can easily be accommodated by changing the generator of the U(1) symmetry such that $U \rightarrow U + ie\alpha[Q, U]$ and $A_\mu \rightarrow A_\mu + \partial_\mu \alpha$ with $Q = \text{diag}(\frac{2}{3}, -\frac{1}{3})$. The standard Skyrme model with the replacement of ∂_μ by $D_\mu = \partial_\mu - ieA_\mu[Q, \cdot]$ remains gauge invariant, although the topological charge density does not and furthermore, it was pointed out by Callan and Witten that this naive gauging of the Skyrme model is not consistent with the anomalies of QCD [6]. The topological charge is not simply fixed by replacing partial derivatives with covariant derivatives, but instead a certain total derivative term must be added, making the entire expression gauge invariant and topological [6]. The Lagrangian, on the other hand, must be amended with some anomalous terms akin to (gauged) Wess-Zumino-Witten terms that are differential 4-forms [6].

The seminal paper [7] by Piette and Tchrakian studies the minimal U(1)-gauged Skyrme model, which is essentially the Skyrme model with partial derivatives replaced by covariant derivatives and the addition of the Maxwell term in the Lagrangian. The model is self-consistent and gauge invariant, but does not reproduce the anomalies of QCD

¹Some ideas in the literature propose that gravity is the gauge theory of diffeomorphisms [4].

as pointed out by Callan and Witten [6]². The gauge prescription of coupling electromagnetism (EM) to the Skyrme model also does more than including just the Coulomb energy in the model. In particular, it turns on a magnetic field that cannot be turned off – even in the neutral solution (corresponding to the neutron). The magnetic field explains also a physical effect, namely the anomalous magnetic moment of the nucleon³. On the other hand, the inclusion of the gauge field – i.e. turning on the magnetic field – reduces the energy of the 1-Skyrmion and it turns out to exacerbate the binding energy problem of the Skyrmions. The worsened binding energy problem for the gauged Skyrmions – a problem that is already severe in the standard Skyrme model – has been considered recently in ref. [13]. In ref. [13] the energy functional is derived from Yang-Mills (YM) calorons, which are YM instantons on $S^1 \times \mathbb{R}^3$, giving rise to two extra terms that are essentially the inner product between the YM field strength as well as its Skyrme field conjugated counterpart and the curvature term $L_\mu L_\nu dx^\mu \wedge dx^\nu$. It is not clear to us, that this is not related to the Wess-Zumino-Witten term of ref. [6] by a total derivative term. Nevertheless, in ref. [13] the couplings and fields are numerically optimized to obtain a much lower energy compared to its lower bound, than was found in the model of ref. [7]. A detailed analysis is needed to conclude whether the model of ref. [13] reproduces the QCD anomalies or not, which could be the case only if there exists a boundary term making this model equal to that of Callan and Witten. A geometric formulation of gauged Skyrmion was later put forward in ref. [14], giving rise to BPS equations whose solutions have vanishing classical binding energies. The incorporation of the pion mass as well as solving the quantum binding energy problem [15] are still issues that need to be tackled in this model of gauged Skyrmions.

U(1) gauged Skyrmions have been studied further in the literature⁴. Refs. [16, 17] like ref. [7] computed the anomalous magnetic moment of the nucleon, but including the Wess-Zumino term that contains the baryon current, hence providing a more physical source for EM. The computation is done for a single $B = 1$ Skyrmion with spherical symmetry, under the assumption that the deformation of the nucleon will be negligible – an assumption not supported by the recent results of ref. [13]. Refs. [16, 17] use the WZ term in the 5-dimensional formulation and it is hence not straightforward to compare with the proposed terms of Callan and Witten [6], although we expect them to be similar, if not identical. The same model has been utilized in ref. [18] to compute the masses and magnetic moments of the neutron and proton under the influence of a strong external magnetic field. The computation is performed with a “spherically symmetric” Ansatz $F(r)$, but in a coordinate system of an ellipsoid, which according to ref. [13] will not suffice for finding true minimizers. Analytic solutions to the massless U(1)-gauged Skyrme equations on a flat box are given in refs. [19–21], although whether such integrable solutions can be made to satisfy physical boundary conditions of a box or whether the solutions represent

² $B = 1$ gauged Skyrmions with the Callan-Witten anomaly terms taken into account were studied recently in ref. [8].

³The inclusion of the nucleon’s spin in this model was done in ref. [9] and the inclusion of the pion mass was done in ref. [10] also for the nucleon ($B = 1$). Skyrmions of higher baryon numbers, i.e. $B = 1$ through 5 were studied in ref. [11]. Gravitating $B = 1$ U(1)-gauged Skyrmions were studied in ref. [12].

⁴There is a volume of literature on SO(3)-gauged Skyrmions and U(1)-gauged baby-Skyrmions (in 2 + 1 dimensions), which we will not discuss here.

the absolute minimum of the energy functional are issues that should be considered with care.

The Skyrme model also comes out as the low-energy effective theory of the holographic Sakai-Sugimoto model [22] (for a review, see ref. [23]), more specifically if all massive vector bosons are decoupled and the effective action is integrated over the holographic direction. This corresponds to taking the holonomy of the instanton as envisioned by Atiyah and Manton [24] and the instanton in the 5-dimensional low-energy effective action is also known as the Sakai-Sugimoto soliton [25]. So one may ask the question: how to take electromagnetism into account in the Sakai-Sugimoto model? To answer this, we need a few more details on the construction. The model is invented to describe the strong interactions, where chiral symmetry and its breaking is geometrically encoded in string theory. That is, the left-handed and right-handed flavours of quarks each have their own D8-brane (i.e. 8 spatial dimensions in its world volume) and these two branes intersect with a D4-brane describing colour degrees of freedom, that is, a string from the D4-brane to the left D8-brane represents a left-handed quark and so on. One dimension of the D4-brane is compactified in order to break the would-be supersymmetry of the superstring theory and the 5 extra dimensions of the D8-branes are assumed to have an $SO(5)$ symmetry. Considering the large- N_c limit, the D8-branes can be viewed as probe branes in the background of the heavy stack of D4-branes, described by the Witten background [26]. The resulting low-energy effective theory is now a 5-dimensional Yang-Mills action for the flavour gauge fields coupled to a 5-dimensional Chern-Simons term, which has the prefactor of the flux of the 5-sphere – the number of colours, N_c . External electromagnetic fields have been considered in such a framework and they are gauge fields living on the D8 flavour branes [27, 28]. It would be very interesting to include dynamics of the electromagnetic fields and reduce the model to the low-energy effective action of the Skyrme model and see whether it would coincide with the gauged Skyrme model of Callan and Witten, especially including the specific gauged Wess-Zumino-Witten-like term.

As evident from the above discussion, the gauging approach of including electromagnetism into the Skyrme model, requires not only a consistent minimal gauging of the Lagrangian, but also the inclusion of a Wess-Zumino-Witten term, that will reproduce the Gell-Mann-Nishijima (GMN) formula for charge, baryon number and isospin. The gauging procedure further turns on a mandatory magnetic flux [7] and strongly deforms the known Skyrmion solutions [13], not to mention the large number of extra couplings between the gauge field and the Skyrme fields. For this reason, we consider here the absolute minimal coupling of the Skyrme model with the Maxwell gauge field with a source dictated by the phenomenological GMN formula. The backreaction to the Skyrme field in this formulation thus happens through the currents of the Skyrme field interacting with the $U(1)$ gauge field. Studying Skyrmons of relatively large baryon number and their deformations due to the backreaction of the Maxwell gauge field is the main purpose of this paper. It is worth noting that this minimal model can be obtained from the Callan-Witten model simply by truncating the Lagrangian to order $\mathcal{O}(e^1)$ (linear order in the electromagnetic coupling). This implies that we neglect the $\mathcal{O}(e\partial A)$ terms in the source for the gauge fields (i.e. $\mathcal{O}(e^2)$ in the Lagrangian) as well as their self interactions, which due to the smallness of the

electromagnetic gauge coupling is physically a quite good approximation.

Studies more similar to our simplistic approach to the problem of Coulomb energy are given in refs. [29–32]. In these cases, the Coulomb energy is computed from the Skyrmion via its baryon charge density and its isospin current. Then the classical technique of expanding the computed charge density in spherical harmonics and then calculating the Coulomb energy as a sum of multipole moments [33], is carried out. In all these papers, no backreaction from the gauge field onto the Skyrme field is taken into account. For small baryon numbers (B of order one), this makes physical sense as the Coulomb energy is small compared to the total mass and hence the backreaction is expected to be small too. This may not be the case when the U(1)-gauged approach is considered though [13].

As evident from the GMN formula, the situation simplifies for two reasons in the isospin-0 cases: The isospin current is not needed and the baryon current becomes simply the baryon density (topological density) of the Skyrmions with all the spatial components vanishing. Two complications arise once a nonvanishing isospin is turned on. The isospin current needs to be normalized, turning the PDEs (partial differential equations) into integro-differential PDEs. Secondly, time-dependence of the Skyrmion turns on nonvanishing spatial components in the baryon current (B^i), which in turn require quantization to be implemented in the equations that need be solved. This thus also turns on a magnetic flux, just as was found in the gauged Skyrme models. We will thus limit ourselves to the isospin-0 case in this paper, but we will take the full backreaction of the Coulomb force into account. We will calibrate the model to physically reasonably chosen observables: the fine-structure constant, the pion mass, the mass and radius of the ^{12}C nucleus, treating F_π and the Skyrme term coupling as free parameters. Finally, since we have fitted the model to physical observables, we expect the backreaction of the Coulomb force to become important near the largest baryon numbers that are stable. Due to our simplification of the problem of treating only the isospin-0 cases, we study Skyrmions with baryon numbers up to $B = 40$, as Calcium-40 is the largest stable $B = 4n$ ($n \in \mathbb{N}$) nucleus. A large number of Skyrmion solutions have been found in ref. [34], so we will use the $B = 4, 8, 12, 16$ solutions as initial conditions for the computations of this paper. For the $B = 40$ Skyrmions, we adopt the same strategy as in ref. [34] i.e. we generate a “large” number of initial conditions that are made of random constellations of $B = 1$ Skyrmions with random orientations in a product Ansatz.

2 The Skyrme model with Coulomb energy

2.1 The field theory

The Lagrangian on base manifold $M = \mathbb{R}^3$ equipped with Minkowski metric η , consisting of the Maxwell term, the Dirichlet (kinetic) term, the Skyrme term, the pion mass term

and the minimal coupling of the gauge field to the electric charge density, reads

$$\begin{aligned} \mathcal{L} = & -\frac{1}{4}F_{\mu\nu}F^{\mu\nu} + \frac{F_\pi^2}{16}\text{tr}(R_\mu R^\mu) + \frac{1}{32g^2}\text{tr}([R_\mu, R_\nu][R^\mu, R^\nu]) + \frac{F_\pi^2 m_\pi^2}{8}\text{tr}(U - \mathbf{1}_2) \\ & - eA_\mu J^\mu, \end{aligned} \quad (2.1)$$

with the electric, baryon, isospin and vectorial currents (all divergenceless)

$$J^\mu = \frac{1}{2}B^\mu + I^\mu \quad (2.2)$$

$$B^\mu = -\frac{1}{24\pi^2}\epsilon^{\mu\nu\rho\sigma}\text{tr}(R_\nu R_\rho R_\sigma), \quad (2.3)$$

$$I^\mu = \frac{(Z - N)J_V^{\mu 3}}{2\int_M J_V^{03}d^3x}, \quad (2.4)$$

$$J_V^{\mu a} = \frac{iF_\pi^2}{16}\text{tr}[(R^\mu - L^\mu)\tau^a] + \frac{i}{16g^2}\text{tr}([(R_\nu, [R^\mu, R^\nu]] - [L_\nu, [L^\mu, L^\nu]])\tau^a), \quad (2.5)$$

the Maxwell field strength $F_{\mu\nu} = \partial_\mu A_\nu - \partial_\nu A_\mu$, the right-invariant and left-invariant chiral currents

$$R_\mu = \partial_\mu U U^\dagger, \quad L_\mu = U^\dagger \partial_\mu U, \quad (2.6)$$

F_π is the pion decay constant, g is the Skyrme coupling constant, m_π is the pion mass, e is the electric charge related to the fine structure constant by $\alpha = \frac{e^2}{4\pi}$ in Heaviside-Lorentz conventions, Z is the number of protons and N is the number of neutrons, and the chiral Lagrangian or Skyrme field U is related to the pions via

$$U = \mathbf{1}_2\sigma + i\tau^a\pi^a, \quad a = 1, 2, 3, \quad (2.7)$$

where τ^a are the standard Pauli spin matrices. The total (integral) electric charge is given by the Gell-Mann-Nishijima formula

$$Q = \frac{1}{2}\int_M (B^0 + 2I^0) d^3x, \quad (2.8)$$

which is the time component of the electric charge current that is coupled to the electromagnetic potential A_μ . Finally, we set the speed of light $c = 1$ and the reduced Planck constant $\hbar = 1$, and use the mostly-positive metric signature.

Although the minimal coupling of the gauge field A_μ to the electric charge current looks gauge variant, it is indeed gauge invariant due to current conservation of the baryon charge current and the isospin charge current

$$A_\mu J^\mu \rightarrow (A_\mu - \partial_\mu\lambda)J^\mu = A_\mu J^\mu - \partial_\mu(\lambda J^\mu), \quad (2.9)$$

up to a total derivative, because

$$\partial_\mu J^\mu = 0, \quad J^\mu := \frac{1}{2}B^\mu + I^\mu, \quad (2.10)$$

is conserved.

The baryon number is the spatial integral of the baryon charge density, which is also the topological degree of the Skyrme field U :

$$B = \int_M B^0 d^3x. \quad (2.11)$$

The number of protons Z and neutrons N in a baryon are related by

$$B = Z + N. \quad (2.12)$$

On the other hand, the isospin I of a nucleus is given by

$$2I = Z - N, \quad (2.13)$$

with the isospin charge

$$I = \int_M I^0 d^3x. \quad (2.14)$$

The Maxwell equations read

$$\partial_\mu F^{\mu\nu} - \frac{e}{2} (B^\nu + 2I^\nu) = 0, \quad (2.15)$$

and it is well known that for static electric charges, the magnetic gauge potential decouples, or in other words: for $B^i = I^i = 0$ we can set $A_i := 0$. For a static Skyrme field ($\partial_0 U = 0$) we have that $B^i = 0$, but $J_V^{i3} \neq 0$. Therefore, the situation drastically simplifies if $Z = N$ yielding $I^i = 0$: that is, the isospin zero case. This case is furthermore simplified, because we do not have to deal with the quantization of the isospin zeromode.

We will focus on the isospin-zero case in the remainder of this paper. Since we have decoupled the magnetic gauge potential (A_i) and work with static Skyrme fields ($\partial_0 U = 0$), we can now simplify the field theory model to

$$\mathcal{L} = \frac{1}{2}(\partial_i A_0)^2 + \frac{F_\pi^2}{16} \text{tr}(R_i^2) + \frac{1}{32g^2} \text{tr}([R_i, R_j]^2) + \frac{F_\pi^2 m_\pi^2}{8} \text{tr}(U - \mathbf{1}_2) - \frac{e}{2} A_0 B^0. \quad (2.16)$$

Since the model is static⁵, the Hamiltonian (energy) is simply minus the Lagrangian

$$E = \int_M \left[-\frac{1}{2}(\partial_i A_0)^2 - \frac{F_\pi^2}{16} \text{tr}(R_i^2) - \frac{1}{32g^2} \text{tr}([R_i, R_j]^2) + \frac{F_\pi^2 m_\pi^2}{8} \text{tr}(\mathbf{1}_2 - U) + \frac{e}{2} A_0 B^0 \right] d^3x. \quad (2.17)$$

It will now be convenient to switch to Skyrme units, by rescaling lengths and energies by $x^i \rightarrow \lambda x^i$ and $E \rightarrow \mu E$, respectively, for which we get the Skyrme units with energies and lengths measured in units of

$$\mu = \frac{F_\pi}{4g}, \quad \lambda = \frac{2}{gF_\pi}, \quad (2.18)$$

⁵The model is static if we treat the electric potential as a scalar field. If we treat it instead as the time-component of a vector field, the Legendre transform will modify the Hamiltonian, but only by a total derivative.

and we are left with the dimensionless energy functional

$$E = \int_M \left[-\frac{\kappa}{2}(\partial_i V)^2 - \frac{1}{2} \text{tr}(R_i^2) - \frac{1}{16} \text{tr}([R_i, R_j]^2) + m^2 \text{tr}(\mathbf{1}_2 - U) + \kappa V B^0 \right] d^3x, \quad (2.19)$$

where we have defined

$$m \equiv \frac{2m_\pi}{gF_\pi}, \quad V \equiv \frac{4}{egF_\pi} A_0, \quad \kappa \equiv \frac{e^2 g^2}{2}. \quad (2.20)$$

The energy functional and hence the (static) theory depends only on two parameters: m and κ (after fixing length and energy units).

For numerical calculations, it will be more convenient to use a 4-vector field ϕ

$$U = \mathbf{1}_2 \phi_0 + i\tau^a \phi_a, \quad a = 1, 2, 3, \quad (2.21)$$

instead of the $SU(2)$ matrix-valued field U . In terms of the $\phi = \{\phi_0, \phi_1, \phi_2, \phi_3\}$ field, the energy functional reads

$$E = \int_M \left[-\frac{\kappa}{2}(\partial_i V)^2 + \partial_i \phi \cdot \partial_i \phi + \frac{1}{2}(\partial_i \phi \cdot \partial_i \phi)^2 - \frac{1}{2}(\partial_i \phi \cdot \partial_j \phi)^2 + 2m^2(1 - \phi_0) + \kappa V B^0 \right] d^3x, \quad (2.22)$$

the baryon charge density now reads

$$B^0 = \frac{1}{12\pi^2} \epsilon_{ijk} \epsilon_{abcd} \partial_i \phi_a \partial_j \phi_b \partial_k \phi_c \phi_d, \quad (2.23)$$

where we adopt the conventions $\epsilon_{123} = \epsilon_{0123} = +1$ and the vector indices $a, b, c, d = 0, 1, 2, 3$.

The equations of motion read

$$\begin{aligned} \partial_i^2 \phi_a - (\phi \cdot \partial_i^2 \phi) \phi_a + (\partial_j \phi)^2 \partial_i^2 \phi_a - (\partial_j \phi)^2 (\phi \cdot \partial_i^2 \phi) \phi_a + (\partial_i \partial_j \phi \cdot \partial_j \phi) \partial_i \phi_a \\ - (\partial_i^2 \phi \cdot \partial_j \phi) \partial_j \phi_a - (\partial_i \phi \cdot \partial_j \phi) \partial_i \partial_j \phi_a + (\partial_i \phi \cdot \partial_j \phi) (\phi \cdot \partial_i \partial_j \phi) \phi_a \\ + \frac{\kappa}{8\pi^2} \epsilon_{abcd} \epsilon_{ijk} \partial_i V \partial_j \phi_b \partial_k \phi_c \phi_d + m^2 (\delta_{a0} - \phi_0 \phi_a) = 0, \end{aligned} \quad (2.24)$$

$$\Delta V = -\partial_i^2 V = B^0. \quad (2.25)$$

Notice that standard variational approaches to minimizing the energy will fail due to the “wrong sign” of the kinetic energy for V . For this reason, we have to use a constrained variational method that we developed in ref. [35].

It will prove convenient to rewrite the Coulomb part of the energy

$$\begin{aligned} E_C &= \int_M \left[-\frac{\kappa}{2}(\partial_i V)^2 + \kappa V B^0 \right] d^3x \\ &= \frac{\kappa}{2} \int_M V (\partial_i^2 V + 2B^0) d^3x \\ &= \frac{\kappa}{2} \int_M (\partial_i V)^2 d^3x \\ &= \frac{\kappa}{2} \int_M V B^0 d^3x, \end{aligned} \quad (2.26)$$

where we have integrated the kinetic term for V by parts and used the equation of motion. The last line in the above equation is numerically easier to evaluate, because for $m \neq 0$, the ϕ fields tend to $(1, 0, 0, 0)$ exponentially, whereas V tends to zero polynomially at spatial infinity. Importantly, the second last line proves that the Coulomb energy is positive semi-definite, which is not *a priori* clear from the energy functional (2.22).

2.2 Geometric approach to the variational problem

The Skyrme energy of a smooth map $\phi : M \rightarrow G$, where $M = \mathbb{R}^3$ is physical space, and $G = \text{SU}(2)$ is target space, is

$$E_{\text{Skyrme}}(\phi) = \int_M \left\{ |\phi^* \mu|^2 + \frac{1}{4} |\phi^* \omega|^2 + f(\phi) \right\}, \quad (2.27)$$

where $\mu \in \Omega^1(G) \otimes \mathfrak{g}$ is the right Maurer-Cartan form on G , $\omega \in \Omega^2(G) \otimes \mathfrak{g}$ is the associated 2-form $\omega(X, Y) = [\mu(X), \mu(Y)]$, $f : G \rightarrow \mathbb{R}$ is a potential function (required to give the pions mass) and we have chosen an $\text{Ad}(G)$ invariant inner product on \mathfrak{g} (namely $\langle X, Y \rangle_{\mathfrak{g}} = -\frac{1}{2} \text{tr}(XY)$). If we interpret ϕ as a static Skyrme field, we should ascribe to it the electric charge density

$$\rho = \frac{1}{2} * \phi^* \Omega, \quad (2.28)$$

where Ω is the volume form on G normalized so that $\int_G \Omega = 1$, and $*$ is the Hodge isomorphism on M . Note that we have implicitly chosen e , the charge of a proton, as our unit of electric charge in making this assertion, and that the total electric charge is $\int_M \rho = B/2$, so that our interpretation of ϕ is consistent only if B is even. Since the field has electric charge, it induces an electrostatic potential $V : M \rightarrow \mathbb{R}$ which is, by definition, the solution of

$$\Delta V = \frac{\rho}{\epsilon_0}, \quad (2.29)$$

satisfying the boundary condition $V(\infty) = 0$. Here $\Delta = -\partial_i^2$ is the Laplacian in the geometer's sign convention and ϵ_0 is the permittivity of free space, a universal physical constant whose numerical value in our coordinate system will depend on our choice of calibration (see later). It follows that the field ϕ induces a Coulomb energy

$$E_C(\phi) = \frac{1}{2} \int_M V \rho, \quad (2.30)$$

and hence that the map $\phi : M \rightarrow G$ corresponding to an isospin 0 nucleus of even baryon number B (consisting of $B/2$ protons and $B/2$ neutrons) is not (as is usually taken) the degree B field that minimizes $E_{\text{Skyrme}}(\phi)$, but rather the degree B field that minimizes

$$E(\phi) = E_{\text{Skyrme}}(\phi) + E_C(\phi). \quad (2.31)$$

The purpose of this section is to derive the first variation formula for this variational problem.

Let ϕ_t be a smooth variation of $\phi = \phi_0 : M \rightarrow G$ of compact support (meaning that $\phi_t(x) = \phi(x)$ for all x outside some compact subset of M), and $\varepsilon = \partial_t \phi_t|_{t=0} \in \Gamma(\phi^{-1}TG)$ its infinitesimal generator (necessarily also of compact support). We seek a formula for the section $\text{grad } E(\phi) \in \Gamma(\phi^{-1}TG)$ which, by definition, for all such variations satisfies

$$\left. \frac{d}{dt} E(\phi_t) \right|_{t=0} = \langle \varepsilon, \text{grad } E(\phi) \rangle_{L^2}. \quad (2.32)$$

A map ϕ is then a critical point of E if $\text{grad } E(\phi) = 0$.

The calculation of $\text{grad } E(\phi)$ is nontrivial principally because $E_C(\phi)$ is a nonlocal functional of ϕ . Indeed, the first variation of $E_{\text{Skyrme}}(\phi)$ is well known [36]:

$$\left. \frac{d}{dt} E_{\text{Skyrme}}(\phi_t) \right|_{t=0} = \left\langle \mu(\varepsilon), 2\delta\phi^*\mu + \frac{1}{2}\delta\xi_\phi + \mu(\nabla f) \right\rangle_{L^2}, \quad (2.33)$$

where $\xi_\phi \in \Omega^1(M) \otimes \mathfrak{g}$ is the \mathfrak{g} -valued one-form

$$\xi_\phi(X) = \sum_i [\phi^*\mu(e_i), \phi^*\omega(X, e_i)], \quad (2.34)$$

$\{e_i\}$ is a local orthonormal frame on M and $\delta = -*d* : \Omega^1(M) \rightarrow \Omega^0(M)$ is the coderivative adjoint to d . Hence

$$\text{grad } E_{\text{Skyrme}}(\phi) = dR_\phi \left\{ \delta \left(2\phi^*\mu + \frac{1}{2}\xi_\phi \right) \right\} + (\nabla f) \circ \phi \quad (2.35)$$

where $R_\phi : G \rightarrow G$ is the right multiplication map $g \rightarrow g\phi$. We note in passing that the formula (2.35) for $\text{grad } E_{\text{Skyrme}}$ is valid on any oriented Riemannian 3-manifold M , for any compact semi-simple Lie group G .

It remains to compute the gradient of

$$E_C(\phi) = \frac{1}{2} \int_{\mathbb{R}^3} V\rho = \frac{\varepsilon_0}{2} \int_{\mathbb{R}^3} V\Delta V. \quad (2.36)$$

Here we must be careful: although the variation of ϕ (and hence of $\phi^*\Omega$) has compact support, V and its induced variation do not. Boundary terms must be treated with care, therefore, and our analysis is restricted to the case of primary interest ($M = \mathbb{R}^3$, $G = SU(2)$). Let us assume that $\phi : M \rightarrow G$ is exponentially spatially localized, in the sense that both $|\phi - \mathbb{I}_2|$ and $|d\phi|$ are exponentially localized, that is, there exists $C > 0$ such that, for all $x \in M$,

$$|\phi(x) - \mathbb{I}_2|, \quad |d\phi_x| \leq C e^{-|x|/C}. \quad (2.37)$$

This condition is natural since the underlying model has massive pions, so we expect the Skyrme field to decay like $e^{-m_\pi|x|}$. Since our variation has compact support, it follows immediately that ϕ_t is also localized in the same sense, and that the electric charge density of ϕ_t , $\rho_t = \frac{1}{2} * \phi_t^*\Omega$ is exponentially spatially localized. A key observation is that the electrostatic potential induced by such a charge distribution is (at least) $1/|x|$ localized:

Lemma 1 *Let $C > 0$ and $\rho : \mathbb{R}^3 \rightarrow \mathbb{R}$ be any smooth function such that $|\rho(x)| \leq Ce^{-|x|/C}$ for all x . Let $V : \mathbb{R}^3 \rightarrow \mathbb{R}$ be the electrostatic potential induced by ρ . Then there exists $K > 0$ such that, for all $x \in \mathbb{R}^3$,*

$$|V(x)| \leq \frac{K}{|x|}, \quad \left| \frac{\partial V}{\partial |x|}(x) \right| \leq \frac{K}{|x|^2}.$$

This follows from elementary estimates on the integral formula for V obtained by Green's function methods, which we present in appendix A.

Let V_t be the potential induced by ρ_t and $\dot{V} = \partial_t \rho_t|_{t=0}$. Denote by B_R the ball in \mathbb{R}^3 centred at 0 of radius R . Then

$$\begin{aligned} \left. \frac{d}{dt} E_C(\phi_t) \right|_{t=0} &= \frac{\varepsilon_0}{2} \int_{\mathbb{R}^3} (\dot{V} \Delta V + V \Delta \dot{V}) \\ &= \lim_{R \rightarrow \infty} \frac{\varepsilon_0}{2} \int_{B_R} (\dot{V} \Delta V + V \Delta \dot{V}) \\ &= \lim_{R \rightarrow \infty} \frac{\varepsilon_0}{2} \left\{ 2 \int_{B_R} V \Delta \dot{V} + \int_{\partial B_R} (V * d\dot{V} - \dot{V} * dV) \right\}, \end{aligned} \quad (2.38)$$

where we have used Stokes's theorem. Now V is induced by ρ , which is exponentially localized, and \dot{V} is induced by $\dot{\rho}$, which has compact support, and hence is also exponentially localized. It follows from Lemma 1 that

$$\lim_{R \rightarrow \infty} \int_{\partial B_R} (V * d\dot{V} - \dot{V} * dV) = 0, \quad (2.39)$$

and hence

$$\left. \frac{d}{dt} E_C(\phi_t) \right|_{t=0} = \varepsilon_0 \int_{\mathbb{R}^3} V \Delta \dot{V} = \int_{\mathbb{R}^3} V \dot{\rho}. \quad (2.40)$$

By the Homotopy Lemma,

$$\dot{\rho} = \frac{1}{2} \partial_t * \phi_t^* \Omega|_{t=0} = \frac{1}{2} * d(\phi^* \iota_\varepsilon \Omega), \quad (2.41)$$

and hence

$$\begin{aligned} \left. \frac{d}{dt} E_C(\phi_t) \right|_{t=0} &= \lim_{R \rightarrow \infty} \frac{1}{2} \int_{B_R} V d\phi^* \iota_\varepsilon \Omega \\ &= \lim_{R \rightarrow \infty} \frac{1}{2} \left\{ \int_{\partial B_R} V \phi^* \iota_\varepsilon \Omega - \int_{B_R} dV \wedge \phi^* \iota_\varepsilon \Omega \right\} \\ &= -\frac{1}{2} \int_{\mathbb{R}^3} dV \wedge \phi^* \iota_\varepsilon \Omega, \end{aligned} \quad (2.42)$$

since ε has compact support.

To extract $\text{grad } E_C$ from eq. (2.42) we note that the normalized volume form at $\mathbb{I}_2 \in G$ is the totally skew-symmetric map

$$\Omega_{\mathbb{I}_2} : \mathfrak{g} \times \mathfrak{g} \times \mathfrak{g} \rightarrow \mathbb{R}, \quad \Omega_{\mathbb{I}_2}(X, Y, Z) = -\frac{1}{4\pi^2} \langle X, [Y, Z] \rangle_{\mathfrak{g}}. \quad (2.43)$$

But Ω is right invariant, so

$$\Omega_g(X, Y, Z) = -\frac{1}{4\pi^2} \langle \mu(X), \omega(Y, Z) \rangle_{\mathfrak{g}}. \quad (2.44)$$

Hence

$$\begin{aligned} *dV \wedge \phi^* \iota_{\varepsilon} \Omega &= (dV \wedge \phi^* \iota_{\varepsilon} \Omega)(e_1, e_2, e_3) \\ &= e_1[V] \Omega(\varepsilon, d\phi(e_2), d\phi(e_3)) + \text{cyclic perms} \\ &= \frac{-1}{4\pi^2} \left\{ e_1[V] \langle \mu(\varepsilon), \phi^* \omega(e_2, e_3) \rangle_{\mathfrak{g}} + \text{cyclic perms} \right\} \\ &= \left\langle \mu(\varepsilon), \frac{-1}{4\pi^2} *dV \wedge \phi^* \omega \right\rangle_{\mathfrak{g}}. \end{aligned} \quad (2.45)$$

It follows that

$$\left. \frac{d}{dt} E_C(\phi_t) \right|_{t=0} = \left\langle \mu(\varepsilon), \frac{1}{8\pi^2} *dV \wedge \phi^* \omega \right\rangle_{L^2}, \quad (2.46)$$

and hence that

$$\text{grad } E_C(\phi) = \frac{1}{8\pi^2} dR_{\phi}(*dV \wedge \phi^* \omega). \quad (2.47)$$

In conclusion, a smooth exponentially localized map $\phi : M \rightarrow G$ is a critical point of $E = E_{\text{Skyrme}} + E_C$ with respect to all smooth variations of compact support if and only if

$$\text{grad } E(\phi) = dR_{\phi} \left\{ \delta \left(2\phi^* \mu + \frac{1}{2} \xi_{\phi} \right) + \frac{1}{8\pi^2} *dV \wedge \phi^* \omega \right\} + (\nabla f) \circ \phi = 0, \quad (2.48)$$

where $V : M \rightarrow \mathbb{R}$ is the unique solution of eq. (2.29). Note that this formula for $\text{grad } E(\phi)$ coincides with (minus two times) the left hand side of (2.24) in the case where $f(\phi) = m^2 \text{tr}(\mathbb{I}_2 - \phi) = 2m^2(1 - \phi_0)$ is the usual pion-mass potential and up to the correct normalization of V .

In order to normalize V correctly, we recall that the energy functional for ϕ (2.27) is defined in ‘‘Skyrme units’’, whereas Gauss’ law is defined with ρ normalized by the charge of the proton. The correct rescaling of V is thus $V \rightarrow \frac{e}{2\lambda} V$, with e being the charge of the proton and λ being the length unit. In order to compute the coupling between the Skyrme field ϕ in Skyrme units and the field V , we need to compare the energy units of the Coulomb energy and the Skyrme energy functional. This amounts to multiplying the Coulomb energy by the length scale and dividing by the energy scale. Combining it all and using that the Coulomb energy contains two V ’s, we have

$$\kappa = \left(\frac{e}{2\lambda} \right)^2 \frac{\lambda}{\mu} = \frac{e^2}{4\mu\lambda} = \frac{e^2 g^2}{2}, \quad (2.49)$$

where in the last step we have used the definitions of the length and energy units of eq. (2.18). Notice that we have recovered the coupling κ of eq. (2.20), which should be inserted in front of the last term in the curly braces of the gradient (2.48).

2.3 Derrick scaling

It is instructive to consider how the Coulomb energy behaves under isotropic dilation of the Skyrme field [37]. That is, for given $\phi : M \rightarrow G$, consider the one-parameter family $\phi_\lambda : M \rightarrow G$, $\phi_\lambda(x) = \phi(\lambda x)$ where $\lambda \in (0, \infty)$. The associated electric charge density is $\rho_\lambda(x) = \lambda^3 \rho(\lambda x)$, so the electrostatic potential V_λ induced by ϕ_λ satisfies

$$-\lambda^2 \sum_{i=1}^3 \frac{\partial^2}{\partial(\lambda x_i)^2} V_\lambda = \frac{\lambda^3}{\epsilon_0} \rho(\lambda x), \quad (2.50)$$

whence we deduce that $V_\lambda(x) = \lambda V(\lambda x)$. Hence, the Coulomb energy of ϕ_λ is

$$E_C(\phi_\lambda) = \frac{1}{2} \int_{\mathbb{R}^3} V_\lambda(x) \rho_\lambda(x) \, d^3x = \frac{\lambda}{2} \int_{\mathbb{R}^3} V(\lambda x) \rho(\lambda x) \, d^3(\lambda x) = \lambda E_C(\phi). \quad (2.51)$$

Defining, as usual, the individual contributions to E_{Skyrme} ,

$$E_2(\phi) = \|\phi^* \mu\|_{L^2}^2, \quad E_4(\phi) = \frac{1}{4} \|\phi^* \omega\|_{L^2}^2, \quad E_0(\phi) = \int_M *f \circ \phi, \quad (2.52)$$

we note that E_C has the same scaling behaviour as E_4 .

Since any static solution of the model is a critical point of $E(\phi)$ for all smooth variations of ϕ , including ϕ_λ , we conclude that such a solution must satisfy the virial identity

$$\begin{aligned} \left. \frac{d}{d\lambda} E(\phi_\lambda) \right|_{\lambda=1} &= \left. \frac{d}{d\lambda} \left\{ \frac{1}{\lambda} E_2(\phi) + \lambda(E_4(\phi) + E_C(\phi)) + \frac{1}{\lambda^3} E_0(\phi) \right\} \right|_{\lambda=1} = 0, \\ &\Rightarrow -E_2(\phi) + E_4(\phi) + E_C(\phi) - 3E_0(\phi) = 0. \end{aligned} \quad (2.53)$$

This provides a useful check on our numerical results. In particular, for fields defined on a bounded box, the variation ϕ_λ is only well-defined for $\lambda \in [1, \infty)$, and minimality of E implies only that $dE(\phi_\lambda)/d\lambda|_{\lambda=1} \geq 0$. Hence, on a bounded domain, the virial identity is replaced by the condition

$$\frac{1}{E(\phi)} \{-E_2(\phi) + E_4(\phi) + E_C(\phi) - 3E_0(\phi)\} \geq 0, \quad (2.54)$$

and the value of this quantity measures the pressure exerted by the box boundary. Of course, one aims to choose the computation domain large enough that this pressure is small. Typical values for the numerical solutions presented below are 0.01-0.08% for ‘‘light’’ Skyrmons, i.e. with baryon numbers in the range [4, 16] and around 0.35% for the large $B = 40$ solutions. The latter rather large pressure suggests that the computational box we have used is on the limit of being big enough, but due to the heavy computational cost of those computations, we have chosen this compromise.

Since E_C scales similarly to E_4 , it is natural to wonder whether Skyrmons can be stabilized by E_C alone, dropping E_4 entirely. Simulations in the $B = 4$ sector suggest that they can, but the model with no Skyrme term is unlikely to be phenomenologically competitive. Our simulations suggest that the electromagnetic coupling (charge) should be about two orders of magnitude larger than experimentally known values, in order to reproduce phenomenologically viable sizes of the nuclei. The stabilization of Skyrmons through electromagnetic interactions alone, with no Skyrme term, was also observed in the gauge-theoretic context in ref. [8].

2.4 Topological energy bound

The Skyrme part of the energy has the topological energy bound given in refs. [38, 39, 34]:

$$E_{\text{Skyrme}} \geq 12\pi^2 \left(\sqrt{\alpha} + \frac{128\sqrt{m}(1-\alpha)^{\frac{3}{4}}\Gamma^2(\frac{3}{4})}{45\pi^{\frac{3}{2}}} \right) |B|, \quad (2.55)$$

with $\alpha \in [0, 1]$:

$$\alpha = \frac{a^2}{2} \left(\sqrt{1 + \frac{4}{a^2}} - 1 \right), \quad (2.56)$$

and finally

$$a = \frac{225\pi^3}{4096m\Gamma^4(\frac{3}{4})}. \quad (2.57)$$

We will shortly calibrate the model and obtain $m \simeq 0.650$, for which $a \simeq 1.162$, $\alpha \simeq 0.6688$ and

$$E_{\text{Skyrme}} \geq 1.088 \times 12\pi^2 |B|. \quad (2.58)$$

Since the Coulomb energy is positive semi-definite, we can infer that the total energy has an energy bound $E \geq E_{\text{Skyrme}}$. It would be interesting to know whether this bound can be improved.

2.5 Numerical algorithm

The numerical algorithm that will be used in this paper is basically that developed in ref. [35]. That is, we perform an arrested Newton flow for the Skyrme field ϕ :

$$P_\phi(\ddot{\phi}) = -\text{grad } E(\phi), \quad (2.59)$$

where $P_\phi : \mathbb{R}^4 \rightarrow T_\phi N$ denotes the orthogonal projection defined by the isometric embedding $N \subset \mathbb{R}^4$, with $N = S^3$ here, and $\text{grad } E(\phi)$ is given in eq. (2.48). The ‘‘arrested’’ part of the Newton flow consists of monitoring the total energy E_ϕ at every step and restarting the flow with vanishing kinetic energy $\dot{\phi} = 0$, if the energy increases. The Coulomb potential V , on the other hand, cannot be solved with the same variational methods, due to its ‘‘wrong sign’’ in the action. For this reason, the numerical algorithm developed in ref. [35], solves the eq. (2.29) or (2.25) completely, at each step of the arrested Newton flow, using the conjugate gradient method. In this sense, the method is a constrained arrested Newton flow where the flow only takes place on trajectories where V is a solution to its governing equation.

An important difference and technical detail, is that the ω_0 field in ref. [35] was massive and hence enjoyed exponential spatial localization, whereas A_0 and hence V in the present paper is massless and obeys a power-law falloff. This makes the accurate evaluation of the total energy at each step of the arrested Newton flow difficult. The solution is simply to use

the Coulomb energy functional written in the last line of eq. (2.26) (see also eq. (2.30)), as opposed to that written in the second to last line. Since the baryon charge B^0 is exponentially spatially localized, so is the integrand VB^0 .

The boundary condition on U : $\lim_{|x| \rightarrow \partial \text{box}} U(x) = \mathbf{1}$ is simple to impose for a sufficiently large box size. In practice, we will instead adopt a Neumann condition on the boundary of the box, since it induces a smaller numerical error in energy and topological charge computations. On the other hand, the boundary condition $\lim_{|x| \rightarrow \infty} V = 0$ is difficult to impose on a finite box, since the power-law falloff is too slow for any manageably sized box. One could attempt to use a complicated Robin boundary condition: $|x|V + \hat{x} \cdot \nabla V = 0$, where the charge needs not be specified. The unspecificity of the charge allows for complicated charge distributions, but these Robin boundary conditions are somewhat tricky to work with for the conjugate gradients method. A much more stable boundary condition, is to assume that the box size is sufficiently large, so that it induces only a small inaccuracy to impose the Dirichlet boundary condition $\lim_{|x| \rightarrow \partial \text{box}} V(x) = \frac{B}{4\pi|x|}$, where B is the total baryon number.⁶ This choice of boundary conditions is very stable, but gives an inaccurate solution for V near the boundary of the box. This inaccuracy is negligible for the energy integral of E_C , due to the strong localization of the electric charge distribution $\rho = eB^0/2$. In this work, we thus work with larger box sizes, i.e. 151^3 lattice sites (sometimes larger) and a lattice distance typically of the order of $h_x \simeq 0.13$, in order to minimize the inaccuracy of the Coulomb energy.

To summarize the numerical algorithm:

1. Perform Newton flow step using Runge-Kutta 4 (RK4).
2. Solve Gauss's equation for V .
3. Compute the total energy and compare with the value of the previous step: If larger, set all kinetic energy to zero.
4. If the residue of the Skyrme field is smaller than a threshold value $\|\text{grad } E(\phi)\|_{L^2}^2 < T$ (T is typically chosen as $T = 10^{-3}$), then stop the algorithm.
5. Continue to the next step (start over).

Our code is implemented in CUDA C and run on a small cluster of NVIDIA GPUs.

2.6 Calibration

Numerically, in Heaviside-Lorentz units, the electric charge is related to the fine-structure constant [40]

$$\alpha = \frac{e^2}{4\pi} \approx \frac{1}{137.036}, \quad (2.60)$$

⁶Notice that the total charge is *not* B , but $eB/2$. However, in the rescaled fields V obeys eq. (2.25). The integral of the right-hand side is B and hence the approximation of V with a point-charge B source is $B/4\pi|x|$ in Heaviside-Lorentz units.

and thus equal to

$$e = 2\sqrt{\pi\alpha} \approx 0.302822. \quad (2.61)$$

The pion masses are given by [40]

$$m_{\pi^\pm} \approx 139.570 \text{ MeV}, \quad m_{\pi^0} \approx 134.977 \text{ MeV}. \quad (2.62)$$

Since we work with unbroken isospin symmetry, we will take the geometric average

$$m_\pi = \sqrt[3]{m_{\pi^\pm}^2 m_{\pi^0}} \approx 138.022 \text{ MeV}. \quad (2.63)$$

In order to calibrate the model, we need two data points of energy and length dimensions, respectively. We will consider the following calibration scheme: We fit the mass and size of the lowest energy $B = 12$ Skyrmion to those of the Carbon-12 nucleus.

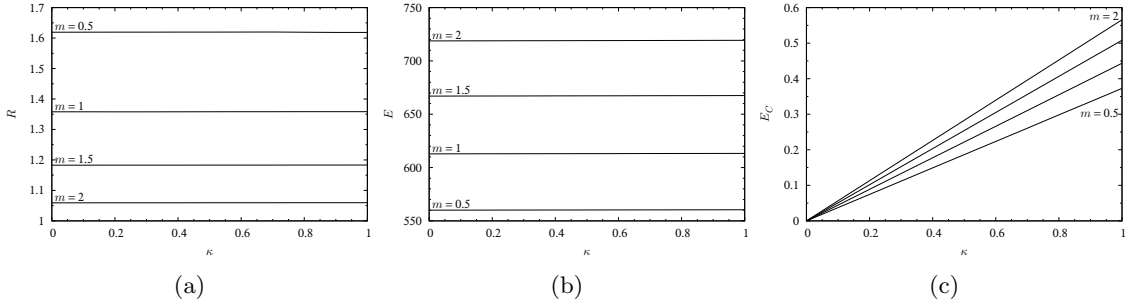


Figure 1: Dependence of the (a) radius, (b) total energy and (c) Coulomb energies on κ in Skyrme units for the $B = 4_a$ cube. The four curves correspond to $m = 0.5, 1, 1.5, 2$, respectively.

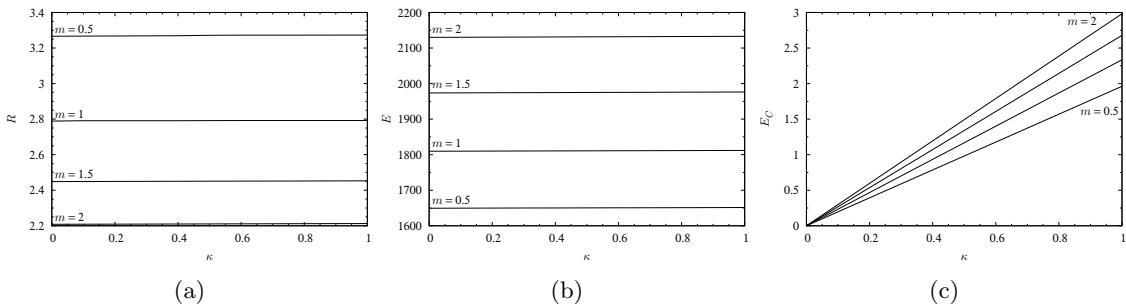


Figure 2: Dependence of the (a) radius, (b) total energy and (c) Coulomb energies on κ in Skyrme units for the $B = 12_a$ chain. The four curves correspond to $m = 0.5, 1, 1.5, 2$, respectively.

In order to see some qualitative dependence on the parameters m, κ for the Skyrmion observables, we plot the radius, the total energy and the Coulomb energy as a function

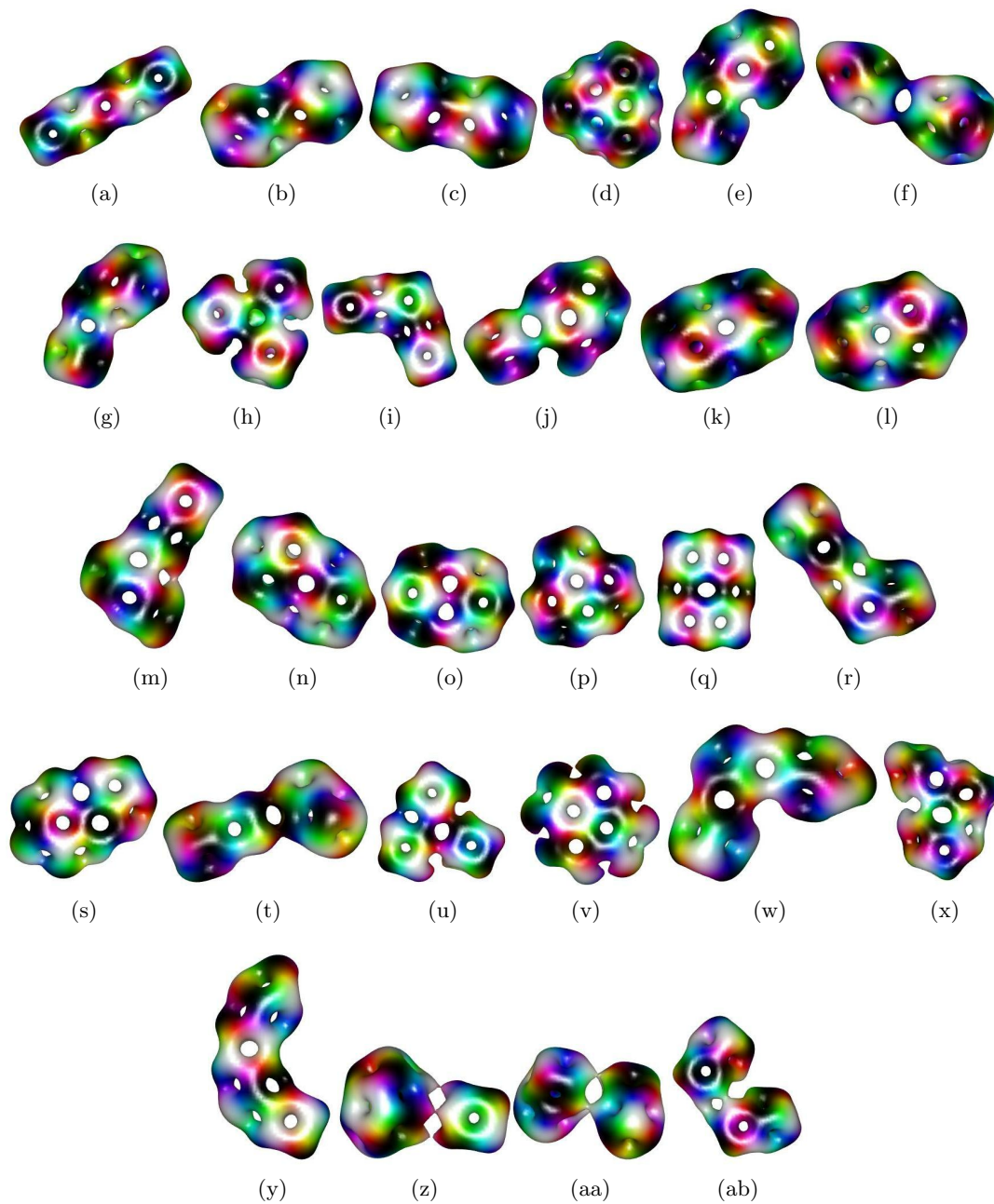


Figure 3: $B = 12$ Skyrmion solutions in order of increasing mass (energy), for $\kappa = 0$ and pion mass $m = 1$. These figures are taken from ref. [34]

of κ for various $m = 0.5, 1, 1.5, 2$ in figs. 1 and 2 for the $B = 4_a$ (cube) and $B = 12_a$ (chain of cubes) Skyrmons, respectively. Clearly the strongest impact on both the radius and the total energy comes from any change in the pion mass parameter, m , whereas the dependence on κ is very mild.

In order to understand which $B = 12$ Skyrmion has the lowest energy as a function of the pion mass, we take all the $B = 12$ Skyrmion solutions of the Smörgårdsbord [34]

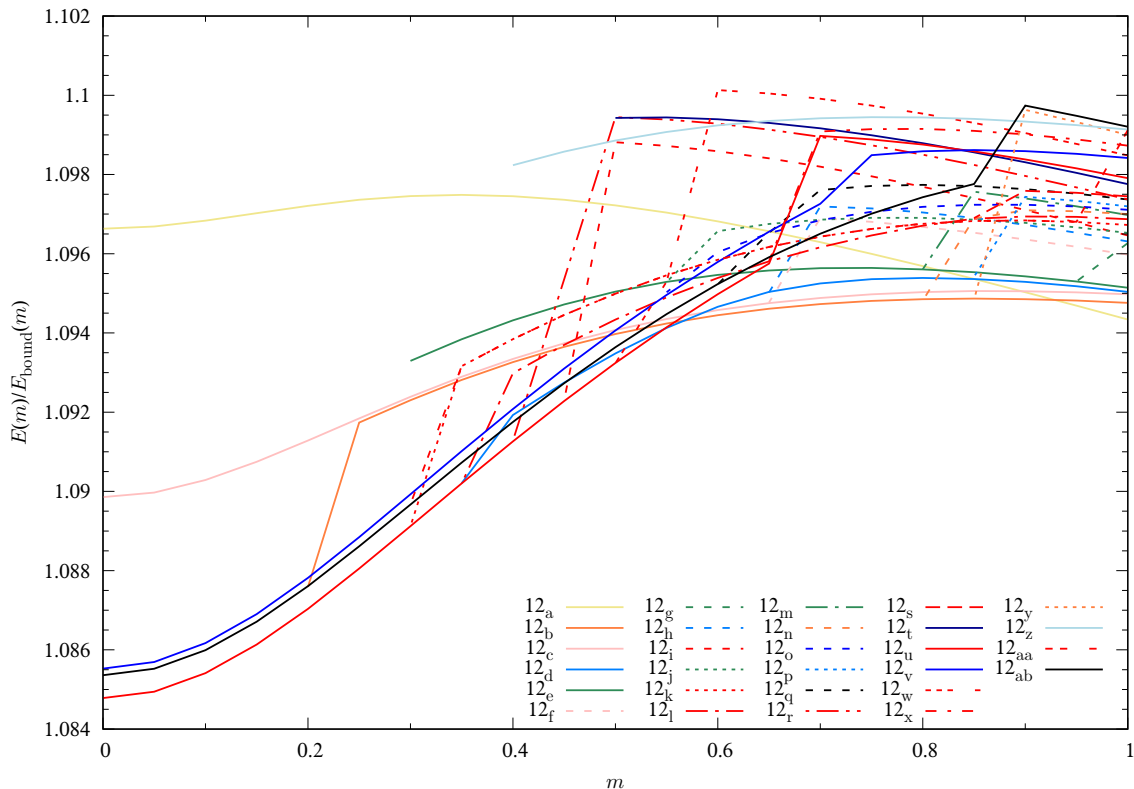


Figure 4: $B = 12$ Skyrmion solutions as functions of the pion mass m for $\kappa = 0$. Since the energy grows drastically with m , we display the energies divided by their topological energy bound, see eq. (2.55). When a curve stops, the solution ceases to exist, but when a curve drops to another existing curve, the solution decays or transforms itself to that solution.

(they are displayed for $m = 1$ and $\kappa = 0$ in fig. 3) and vary the pion mass parameter in the range $m \in [0, 1]$, which *a posteriori* turns out to be sufficient for calibrating the theory. For Skyrmion number $B = 12$ and in particular for the most stable $B = 12$ Skyrmons, the backreaction of the Coulomb energy has a nearly negligible impact, see fig. 2. The energy of all the $B = 12$ solutions of fig. 3 are shown in fig. 4 as functions of their pion mass parameter, m , for $\kappa = 0$. When a curve stops, the solution ceases to exist, but when a curve drops to another existing curve, the solution decays or transforms itself to that solution. Hysteresis is existing, but is negligible and comparable to the slope of the curves transitioning between solutions.

Ignoring for the moment the backreaction of the Coulomb energy, we can read off the stable $B = 12$ Skyrmion solutions in the interval $m \in [0, 1]$, which we illustrate in fig. 5. It turns out that the chain of 3 alpha particles is only the ground state of the $B = 12$ sector for large pion mass, near $m \sim 1$, whereas the relevant Skyrmion for a more realistic pion mass is made of two $B = 7$ Skyrmons sharing a face. We also checked explicitly, that turning on a finite κ of order one, does not change the ground states (global energy minimizers). The evolution of the solutions as functions of the pion mass parameter m

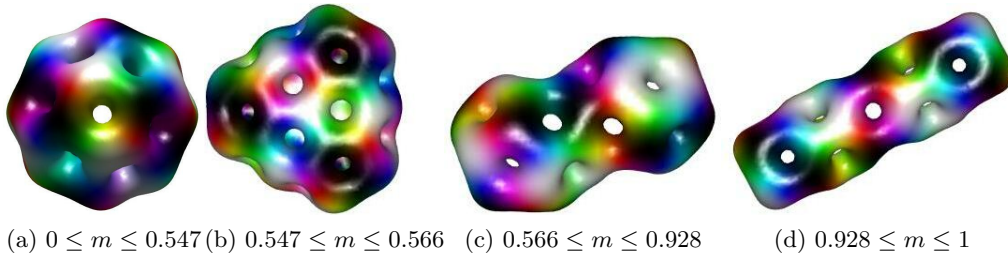


Figure 5: Stable $B = 12$ Skyrmion solutions (global energy minimizers) for $\kappa = 0$ and pion mass in the interval $m \in [0, 1]$.

for $\kappa = 0$ is shown in fig. 6.

Fitting now the mass and radius of the $B = 12$ ground state to the mass and radius of the ^{12}C nucleus, we have [41, 40]

$$\begin{aligned} \frac{F_\pi}{4g} E_{12}(m, \kappa) &= M_{12\text{C}} \approx 11177.9 \text{ MeV}, \\ \frac{2}{gF_\pi} R_{12}(m, \kappa) &= R_{12\text{C}} \approx 2.4702 \text{ fm} \approx 1.2518 \times 10^{-2} \text{ MeV}^{-1}. \end{aligned} \quad (2.64)$$

The charge radius of a Skyrmion in Skyrme units is calculated as

$$R_B = \sqrt{\frac{1}{B} \int_M r^2 B^0 d^3x}, \quad (2.65)$$

with $r \equiv |x - x_0|$ being the radial distance from the centre of the charge distribution, x_0 , which is calculated as

$$x_0^i = \frac{1}{B} \int_M x^i B^0 d^3x, \quad i = 1, 2, 3. \quad (2.66)$$

We will now perform the calibration of the model, by computing the mass as a function of m and κ , and it suffices to consider the $B = 12_b$ Skyrmion of fig. 5(c), which is the union of two $B = 7$ Skyrmons with icosahedral symmetry that share a face. The result of the calibration is

$$m \simeq 0.650, \quad \kappa \simeq 0.737, \quad (2.67)$$

for which the Skyrme coupling constant and the pion decay constant read

$$g \simeq 4.010, \quad F_\pi \simeq 105.9 \text{ MeV}, \quad (2.68)$$

both of which are smaller than those obtained by Adkins-Nappi-Witten using a fit of the nucleon and the Delta resonance (both are $B = 1$ Skyrmons) [42], but both values are larger than those fitted to Lithium-6 in ref. [43, eq. (77)].

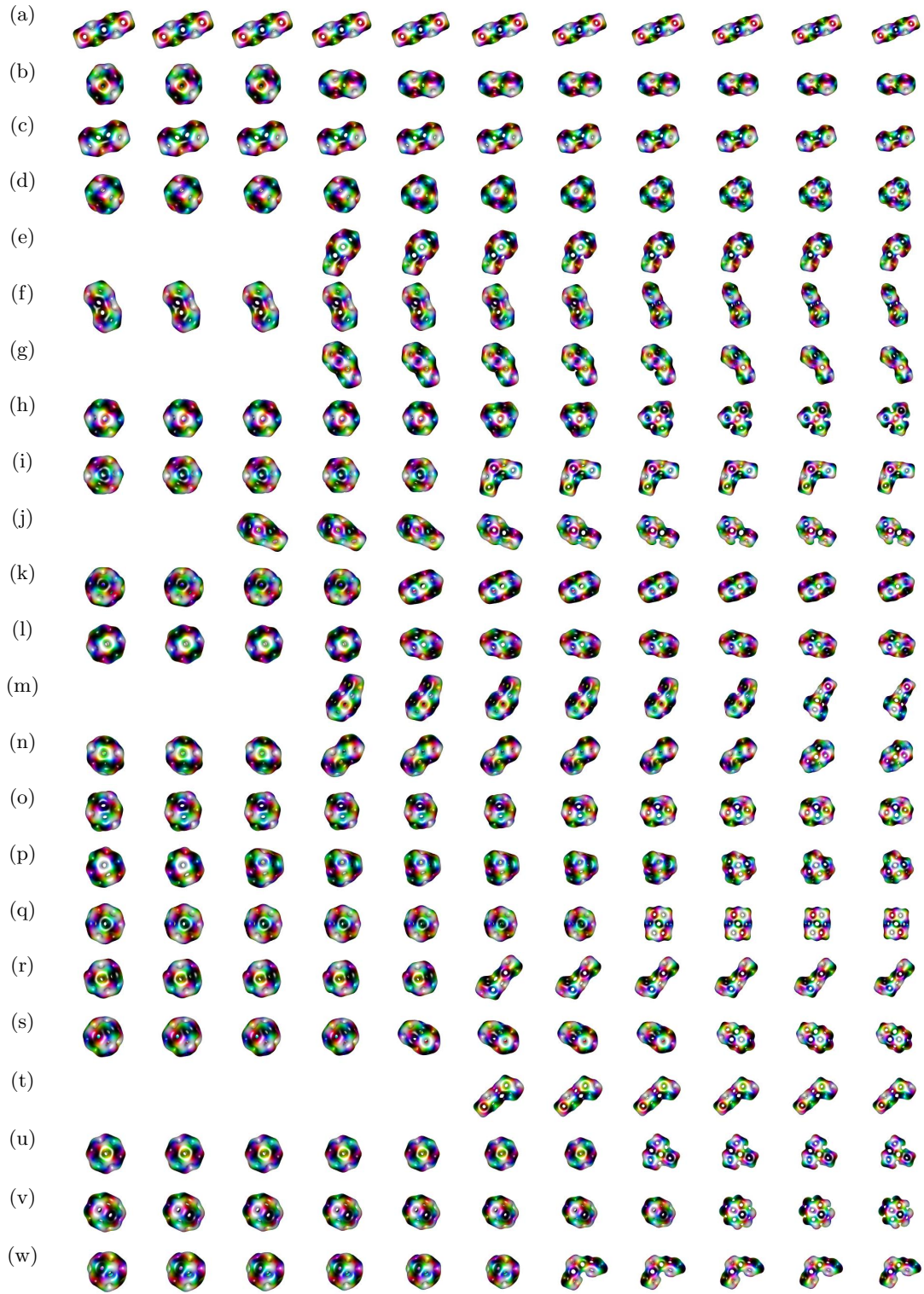


Figure 6: The evolution of $B = 12$ Skyrmion solutions of fig. 3 as functions of the pion mass for $\kappa = 0$, which is lowered from $m = 1$ (right-most column) to $m = 0$ (left-most column). The steps in m between each column is twice as large as compared to those shown in fig. 4.

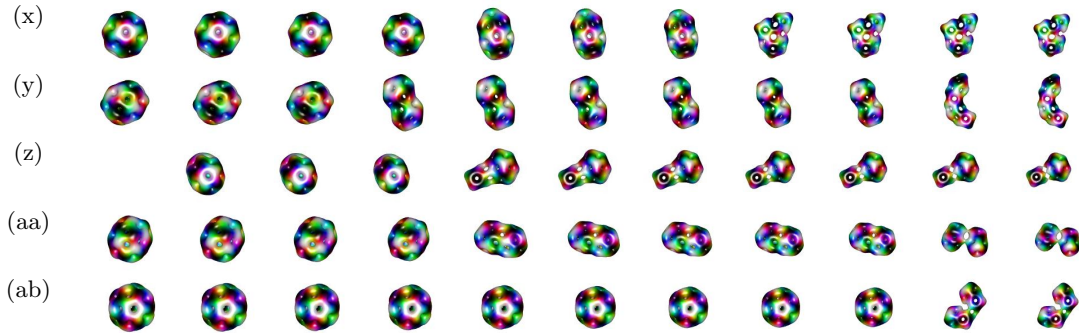


Figure 6: This figure is continued from the previous page.



Figure 7: The $B = 4$ Skyrmion.

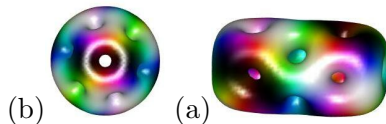


Figure 8: The two existing $B = 8$ Skyrmion solutions at $m = 0.65$. The 8_b -Skyrmion is the lightest in our calibration.

2.7 Skyrmion solutions

We will now present the numerical Skyrmion solutions. The 4-Skyrmion is unaltered and is still a cube, see fig. 7. The 8-Skyrmions have reduced from 4 solutions in ref. [34] to only the two lightest solutions, see fig. 8. The lightest 8-Skyrmion at $m = 1$ is the 8_a solution, which becomes the next-lightest one at $m = 0.65$, whereas the 8_b solution becomes the lightest state. No apparent effect is visible from the Coulomb energy with full backreaction (for details on the impact of the Coulomb force, see the next section); that is, the 2 heavier 8-Skyrmions that were a 7-Skyrmion with a 1-Skyrmion and a 6-Skyrmion with a torus mounted on the side instead of at the end, have both disappeared due to the lower pion mass, but with and without the Coulomb backreaction taken into account they both decay to the lightest 8_b Skyrmion.

Let us turn to the $B = 12$ Skyrmions. We start with listing the changes to the solutions due to changing the fit of the model from $m = 1$, $\kappa = 0$ to $m = 0.65$, $\kappa = 0.737$, see tab. 1. In the previous section, the EM interactions were not taken into account. Here we compute the new solutions with $m = 0.65$ with and without the EM interactions turned on; in both cases starting with the $m = 1$, $\kappa = 0$ solution as the initial condition. The new solutions that appear in the process are shown in fig. 9. The four cases where the Skyrmions flow to two different solutions for the Coulomb backreaction turned off ($\kappa = 0$) and on ($\kappa = 0.737$), are shown in fig. 10. The 12_f -Skyrmion remains the 12_f -Skyrmion when the Coulomb force

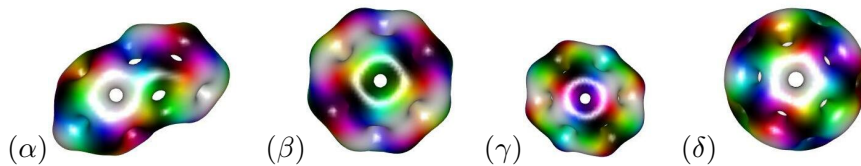


Figure 9: $B = 12$ Skyrmion solutions that are new compared with the solutions of the Smörgåsbord [34]. Since these solutions are computed for the pion mass $m = 0.65$, they may not exist for $m = 1$.

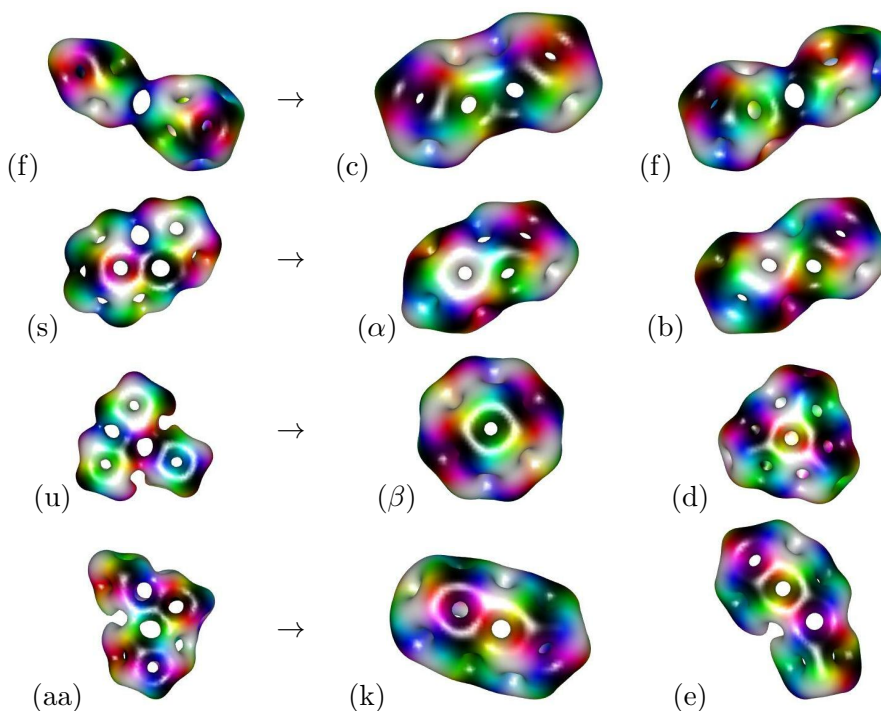


Figure 10: $B = 12$ Skyrmions that differ when the electromagnetic interactions are taken into account. The left-most column shows the initial conditions with $m = 1$, $\kappa = 0$, the middle column shows the solutions for $m = 0.65$, $\kappa = 0$ and the right-most one is for $m = 0.65$, $\kappa = 0.737$.

config ($m = 1$)	$\kappa = 0$ ($m = 0.65$)	$\kappa = 0.737$ ($m = 0.65$)	config ($m = 1$)	$\kappa = 0$ ($m = 0.65$)	$\kappa = 0.737$ ($m = 0.65$)
12_f	12_c	* 12_f	12_s	12_α	* 12_b
12_g	12_e	12_e	12_u	12_β	* 12_d
12_h	12_d	12_d	12_v	12_γ	12_γ
12_m	12_e	12_e	12_x	12_l	12_l
12_n	12_b	12_b	12_y	12_b	12_b
12_p	12_d	12_d	12_{aa}	12_k	* 12_e
12_q	12_o	12_o	12_{ab}	12_δ	12_δ

Table 1: $B = 12$ Skyrmions' change from $m = 1$, $\kappa = 0$ to the physical fit of $m = 0.65$ with and without the physical EM coupling, $\kappa = 0.737$, turned on. The red entries denote solutions that differ from the $m = 1$ ones, whereas the * denotes solutions that are different when the electromagnetic interactions are taken into account compared with when it is turned off. Skyrmions with Greek indices are new compared to the $m = 1$, $\kappa = 0$ case. Skyrmions that remain unaltered are not shown in this table.

is turned on, but changes to the 12_c -Skyrmion with $\kappa = 0$. The 12_s - and 12_u -Skyrmions flow to two new Skyrmion solutions when $\kappa = 0$ and m is lowered from $m = 1$ to $m = 0.65$, which are denoted 12_α - and 12_β -Skyrmions, respectively. Finally, the 12_{aa} -Skyrmion flows to two different existing solutions, upon changing the pion mass and including the EM interaction or not. The remaining ten Skyrmions in tab. 1 all flow to the *same* Skyrmion

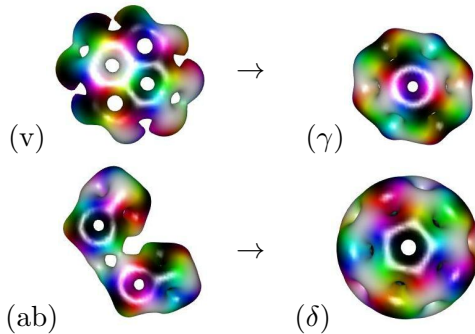


Figure 11: $B = 12$ Skyrmions that flow to the same *new* Skyrmion solution due to the change of the pion mass $m = 1 \rightarrow 0.65$, independently of whether the Coulomb force is turned on or not. The left-most column shows the initial conditions with $m = 1$, $\kappa = 0$, whereas the right-most column shows the $m = 0.65$, $\kappa = 0.737$ case. The $m = 0.65$, $\kappa = 0$ solutions are the same as the $\kappa = 0.737$ ones.

solution upon changing the pion mass from $m = 1$ to $m = 0.65$, independently of whether the Coulomb force is turned on or not. In most cases, the Skyrmion flows to an existing lower-energy solution. However, in two cases, the Skyrmion flows to a new solution. These two cases are shown in fig. 11.

Finally, we show in fig. 12 the ten lightest $B = 12$ Skyrmion solutions in our calibration (pion mass $m = 0.65$) without taking the Coulomb force into account (left-hand side) and with taking it into account (right-hand side). It is interesting to note that the expected

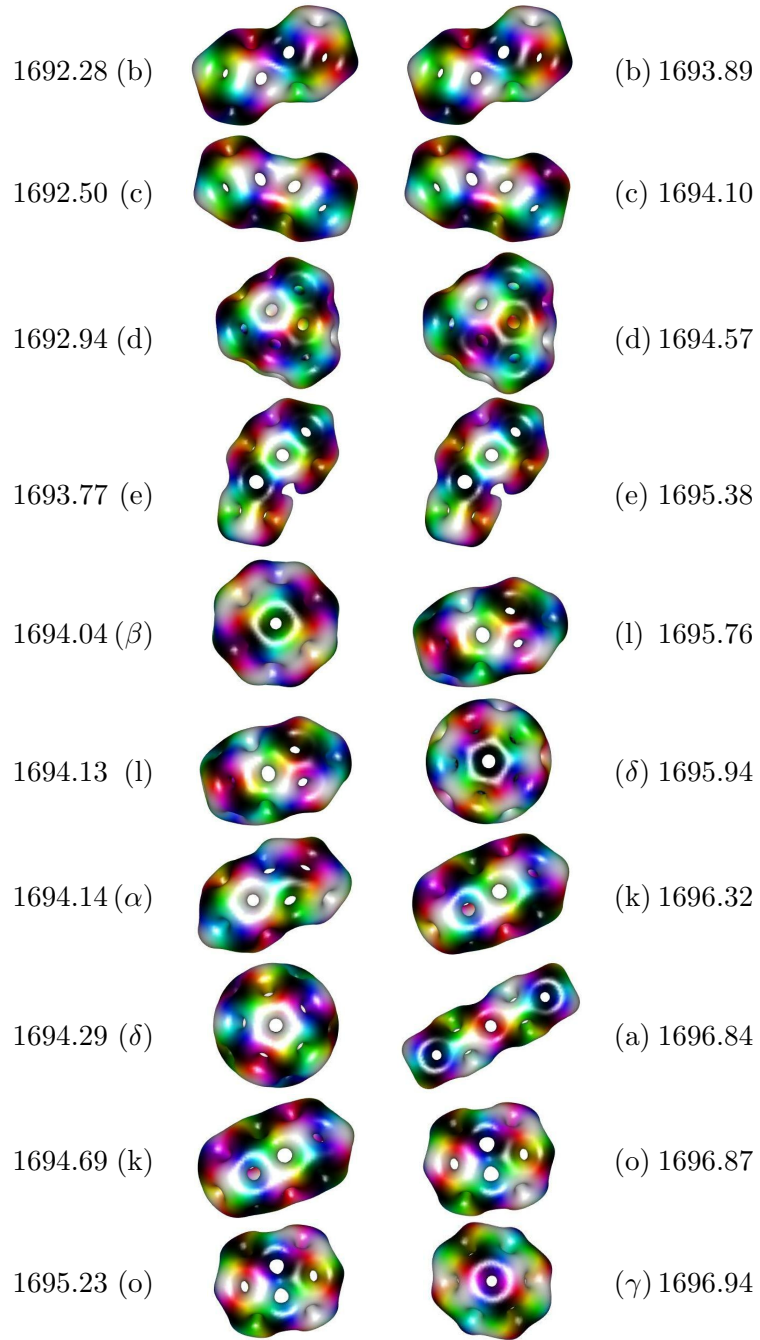


Figure 12: The ten lightest $B = 12$ Skyrmion solutions with $m = 0.65$ without Coulomb backreaction (left-hand side) and with the Coulomb backreaction taken into account (right-hand side). The solution labels refer to the solutions of figs. 3 and 9. Interestingly, the 12_a solution that is a chain of three cubes, is not the global energy minimizer in our calibration.

global energy minimizer (ground state), i.e. the chain of three cubes (alpha particles), turns out not to be the minimizer in our calibration. Not only is it not the minimizer, it is not even in the top-ten lightest states when the Coulomb backreaction is turned off ($\kappa = 0$), whereas it figures as the 8th lightest state when it is taken into account. The four lightest states turn out to be the same, whether EM interactions are backreacted or not. In particular, the ground state for $B = 12$ is the same solution: namely the 12_b -Skyrmion solution made up of two icosahedrally symmetric Skyrmons that share a face.

We now turn to the rather large ensemble of Skyrmons, i.e. the $B = 16$ sector of the Smörgåsbord [34]. As one could expect from the results in the $B = 12$ sector, the alterations in this sector will be even more. Due to the large number of $B = 16$ solutions, we do not display all the known solutions and refer to the labels of the solutions used in ref. [34] using the Latin alphabet. The new $B = 16$ solutions are denoted using the Greek alphabet (skipping omicron, since it looks like 'o'). We start by listing a table of the changes that happen when using the $B = 16$ Skyrmons as initial conditions for our calibration, i.e. with pion mass $m = 0.65$ with and without taking into account the backreaction of the Coulomb force, see tab. 2.

There are 9 cases, where the Skyrmon solution disappears; this can happen for example by the smaller pion mass not squeezing the Skyrmon as much at $m = 0.65$ as compared with at $m = 1$ and hence several Skyrmons inflate to the same more hollow solution. Other possibilities include that the Skyrmon solution simply breaks up into smaller chunks and hence does not count as a $B = 16$ solution.

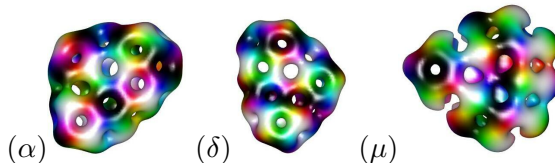


Figure 13: New $B = 16$ Skyrmon solutions that were found with Coulomb backreaction taken into account ($m = 0.65$ and $\kappa = 0.737$). In all these cases, the Skyrmon solution found without the Coulomb force turned on was a known one. In the case of the 16_μ -Skyrmion, the known solution was the same as the initial condition (16_{dn}).

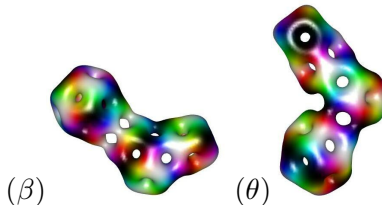


Figure 14: New $B = 16$ Skyrmon solutions that were found with Coulomb backreaction taken into account ($m = 0.65$ and $\kappa = 0.737$). In all these cases, no $B = 16$ solution was found when the Coulomb force was not included.

There are furthermore 15 cases, where the solutions are different when the Coulomb backreaction (CBR) is taken into account from when it is not. In 3 of the 15 cases, the

config ($m = 1$)	$\kappa = 0$ ($m = 0.65$)	$\kappa = 0.737$ ($m = 0.65$)	config ($m = 1$)	$\kappa = 0$ ($m = 0.65$)	$\kappa = 0.737$ ($m = 0.65$)
16_i	–	–	16_{cj}	16_η	16_η
16_k	16_a	16_a	16_{cl}	16_p	16_p
16_m	16_c	16_c	16_{cn}	16_c	16_c
16_o	–	$*16_o$	16_{co}	16_a	16_a
16_t	16_c	$*16_\alpha$	16_{cr}	–	$*16_{cp}$
16_z	–	–	16_{cs}	–	$*16_\theta$
16_{ae}	–	$*16_\beta$	16_{cu}	–	–
16_{ai}	–	$*16_{aa}$	16_{cv}	16_a	$*-$
16_{av}	–	–	16_{cy}	–	$*16_{cy}$
16_{ax}	16_γ	16_γ	16_{cz}	16_ι	16_ι
16_{ay}	–	–	16_{da}	16_κ	16_κ
16_{az}	16_c	16_c	16_{dd}	–	$*16_{dd}$
16_{bb}	16_c	$*16_\delta$	16_{de}	16_{aa}	16_{aa}
16_{bc}	16_y	16_y	16_{dg}	16_λ	16_λ
16_{bd}	–	–	16_{dn}	16_{dn}	$*16_\mu$
16_{bf}	16_ε	16_ε	16_{do}	16_ν	16_ν
16_{bj}	16_c	16_c	16_{dp}	–	–
16_{bl}	16_c	16_c	16_{du}	16_c	16_c
16_{bm}	–	$*16_p$	16_{dx}	16_c	16_c
16_{bq}	–	–	16_{eb}	–	–
16_{bs}	16_l	$*16_d$	16_{ec}	16_ξ	$*16_p$
16_{bu}	16_s	16_s	16_{eh}	16_π	16_π
16_{bx}	16_c	16_c	16_{ej}	16_{dy}	16_{dy}
16_{ce}	16_ζ	16_ζ	16_{em}	16_{bw}	16_{bw}
16_{ci}	16_c	$*16_{ci}$	16_{eo}	16_ρ	16_ρ

Table 2: $B = 16$ Skyrmions' change from $m = 1$, $\kappa = 0$ to the physical fit of $m = 0.65$ with and without the physical EM coupling, $\kappa = 0.737$, turned on. The – denote solutions that do not exist, the red entries denote solutions that differ from the $m = 1$ ones, whereas the * denotes solutions that are different when the electromagnetic interactions are taken into account compared with when it is turned off. Skyrmions with Greek indices are new compared to the $m = 1$, $\kappa = 0$ case. Skyrmions that remain unaltered are not shown in this table.

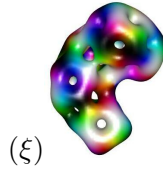


Figure 15: New $B = 16$ Skyrmion solution found by changing to our calibration, but without the Coulomb backreaction ($m = 0.65$ and $\kappa = 0$). Turning on the Coulomb backreaction gave a different, albeit known Skyrmion solution (16_p).

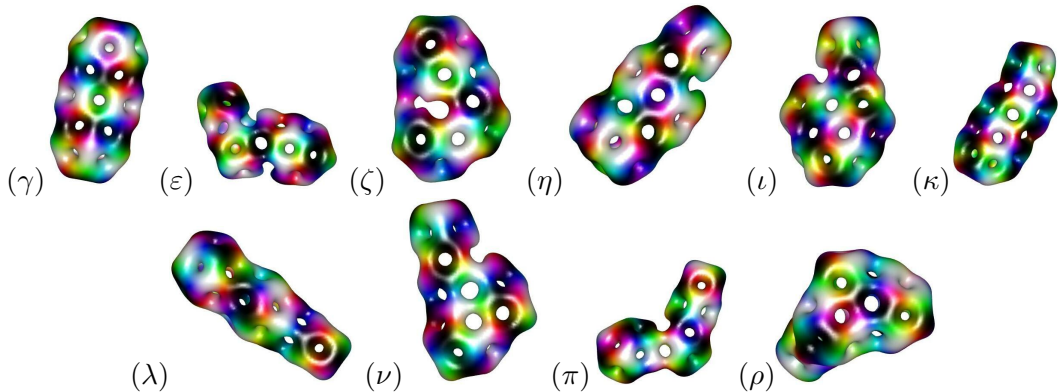


Figure 16: New $B = 16$ Skyrmion solutions found by changing to our calibration, but the solutions are qualitatively the same with and without the Coulomb backreaction taken into account. The figure shows the solutions for $m = 0.65$ and $\kappa = 0.737$.

Skyrmion remained the same with the Coulomb backreaction turned on, but disappeared when it was switched off and in 1 case, it remained with the backreaction (16_{ci}), but changed to a low-energy solution when it was turned off (16_c). Only in one case, did the Skyrmion solution disappear with CBR turned on and in this case (16_{cv}) the solution without CBR decayed to one of the lowest-energy solutions (16_a). This may suggest that the Skyrmion solutions are more stable with the CBR taken into account. In 3 cases, a new Skyrmion solution was found when CBR was taken into account, whereas the solution flowed to a known solution without CBR; in one of these cases, the solution without CBR remained the same, see fig. 13. In 2 cases, the new Skyrmion solution was found with CBR taken into account, whereas no solution exists without it, see fig. 14. In further 3 cases, no solution exists without the CBR taken into account, but with CBR the solution flowed to a different, albeit known Skyrmion solution, see tab. 2. In one case, the solutions flowed to 2 different known solutions. Finally, in one case a new Skyrmion solution was found without the CBR taken into account, whereas it flowed to a known solution (16_p) with it, see fig. 15.

We now conclude the $B = 16$ sector by showing the ten lightest Skyrmion solutions in our calibration (pion mass $m = 0.65$) in fig. 17, without taking the CBR into account (left-hand side) and with it (right-hand side). Unlike the case of the $B = 12$ Skyrmons, the ten lightest $B = 16$ Skyrmons are the same whether CBR is taken into account or not. Interestingly though, there appears a new Skyrmion as 16_γ as the 6th lightest Skyrmion in our calibration. The ground state is however the same 16_a solution as in ref. [34].

For the $B = 40$ Skyrmons, we seed the computations with 60 random configurations using the algorithm of ref. [34] and run the arrested Newton flow to a final solution with and without the Coulomb energy backreacted to the Skyrme fields. First some statistics. We find that 15 of them come out equal. 5 of them do not give rise to solutions with $B = 40$ without taking the Coulomb effect into account, but do flow to solutions when its backreaction is taken into account. Of these 5 solutions, using the final solutions as input, in 1 case the solution is equal when the Coulomb effect is turned off and in another

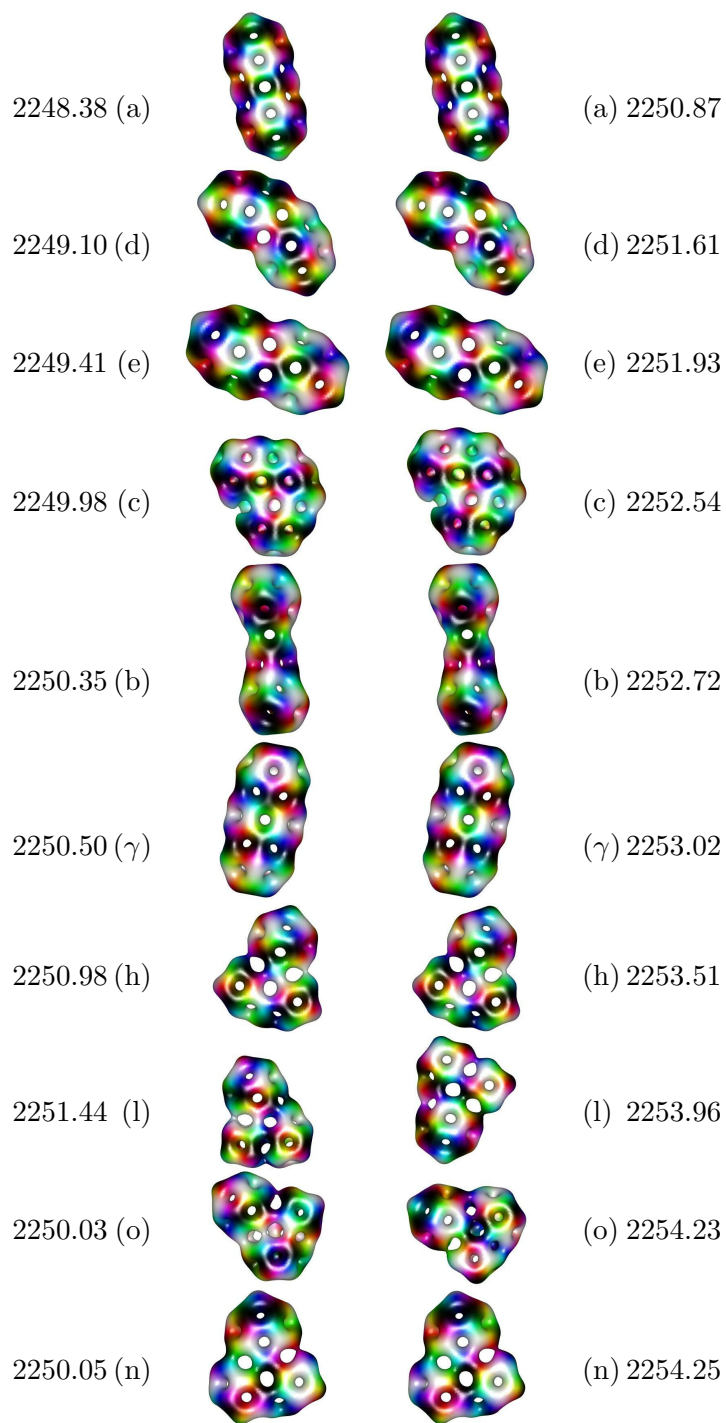


Figure 17: The ten lightest $B = 16$ Skyrmion solutions with $m = 0.65$ without Coulomb backreaction (left-hand side) and with the Coulomb backreaction taken into account (right-hand side). The solution labels refer to the solutions of ref. [34] and γ refers to the new Skyrmion solution of fig. 16. In this sector, all the ten lightest Skyrmions are the same with and without the Coulomb backreaction taken into account.

the solution changes; finally, in 3 cases the solution ceases to exist (with baryon number 40). The remaining 40 solutions come out different; that is, starting with the same random initial configuration of 1-Skyrmions placed randomly, the arrested Newton flow algorithm find two *different* solutions when taking into account the backreaction of the Coulomb force and when not taking it into account. However, in 37 of these 40 cases, even though they flow to different solutions, taking each of these final solutions as input, they both exist when respectively turning off or switching on the Coulomb force. In 2 cases, the solution ceases to exist (with baryon number 40) when the Coulomb force is switched off. Finally, in 1 single case, interestingly, the solution without the Coulomb effect taken into account flows to the same solution from that without it taken into account once the Coulomb force is turned on.

This rather limited statistical sample shows that, although the Coulomb effect is somewhat small, it does have physical importance for the existence of certain Skyrmion states, but it appears that it is more important for the *dynamics* of nuclei. We note, however, that the dynamics here is not quite the physical dynamics, as the arrested Newton flow artificially removes the kinetic energy to speed up the process of finding a minimum of the static energy (although this removal of kinetic energy somehow crudely mimics energy being carried away by radiation).

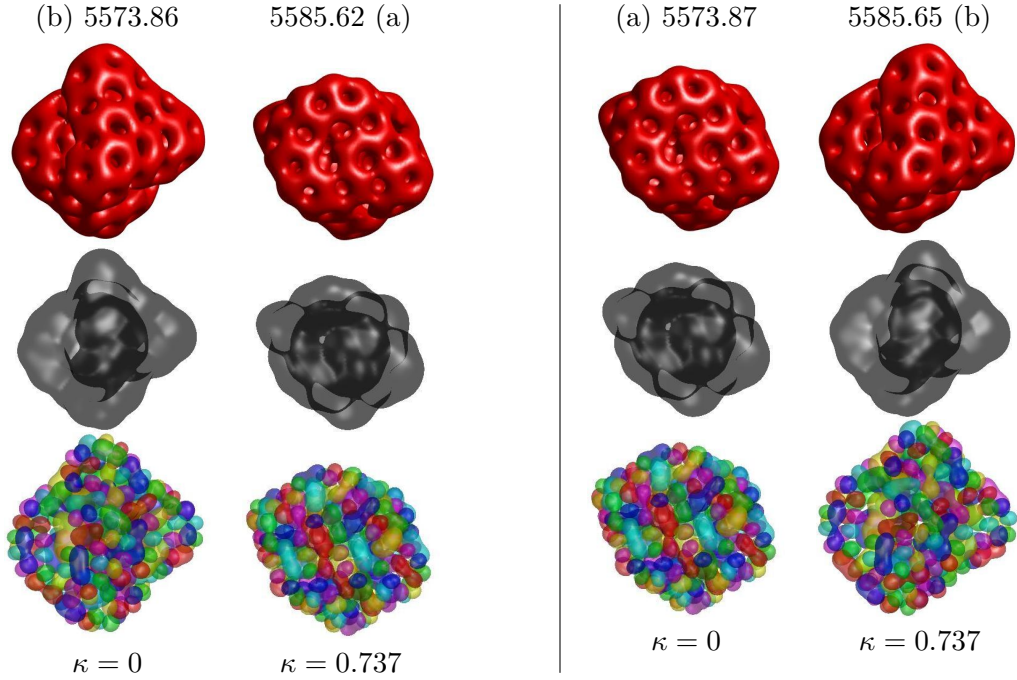


Figure 18: The lightest (left) and next-to-lightest (right) $B = 40$ Skyrmions. The three rows displays the baryon charge isosurface at $1/4$ of the maximum density, the $\sigma = \phi_0$ isosurface at $\phi_0 = 0$ and the pion isosurfaces with $\phi_{1,2,3} = 3/4$ ($\phi_{1,2,3} = -3/4$) corresponding to red, green, blue (cyan, magenta, yellow). The labels of $B = 40$ Skyrmion solutions are ordered according to the energies of the Coulomb backreacted solutions (i.e. those with $\kappa = 0.737$).

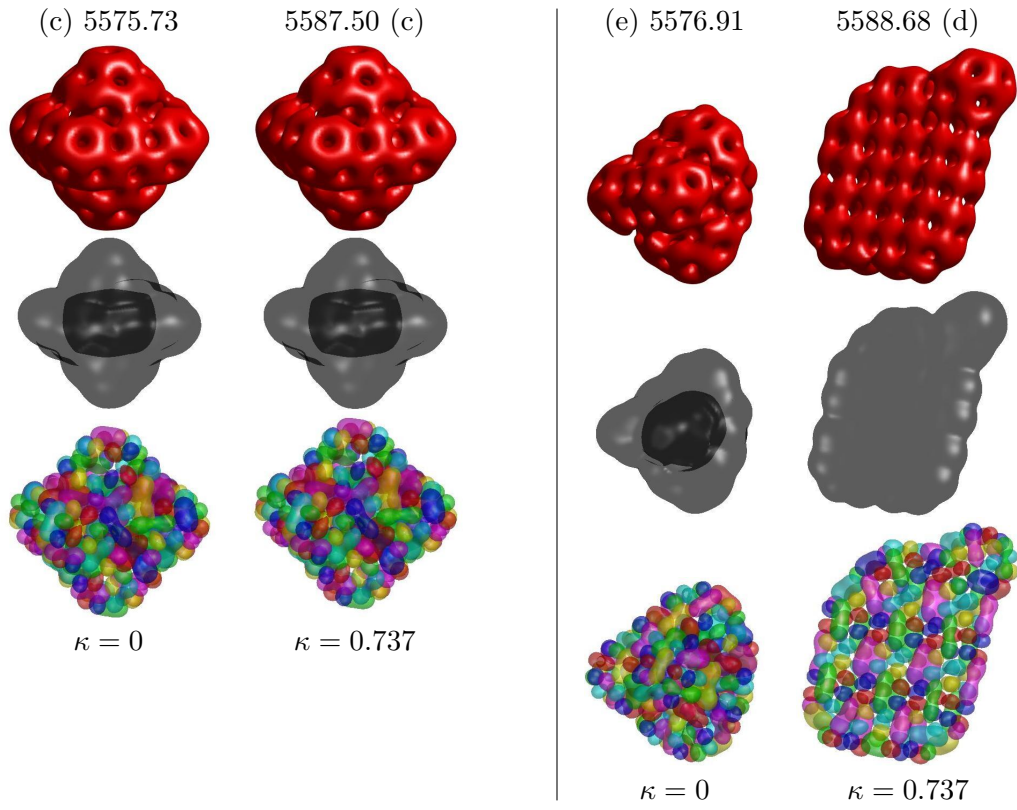


Figure 19: The 3rd (left) and 4th (right) lightest $B = 40$ Skyrmions. For details, see the caption of fig. 18.

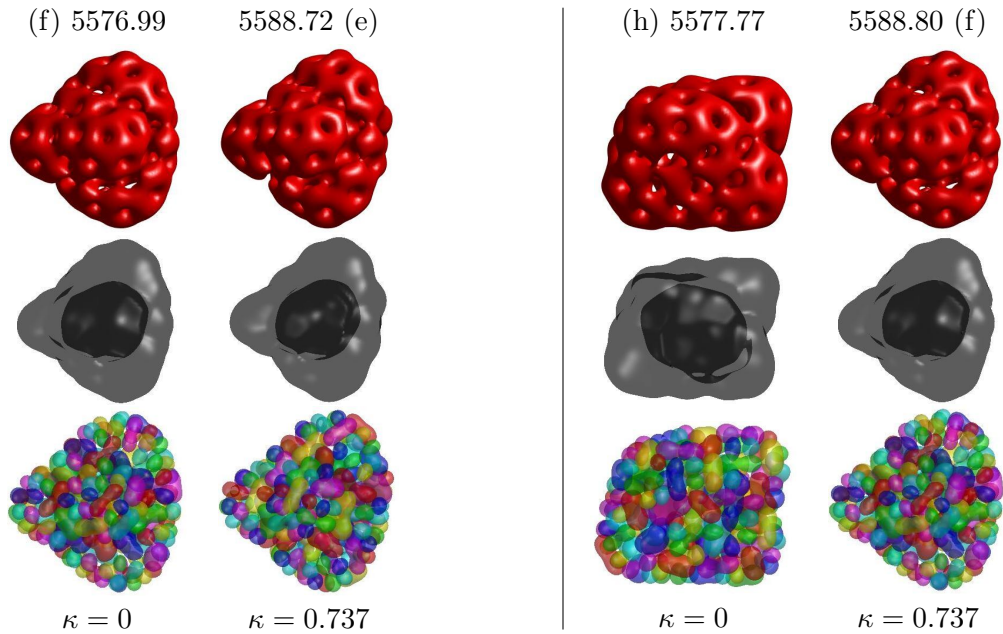


Figure 20: The 5th (left) and 6th (right) lightest $B = 40$ Skyrmions. For details, see the caption of fig. 18.

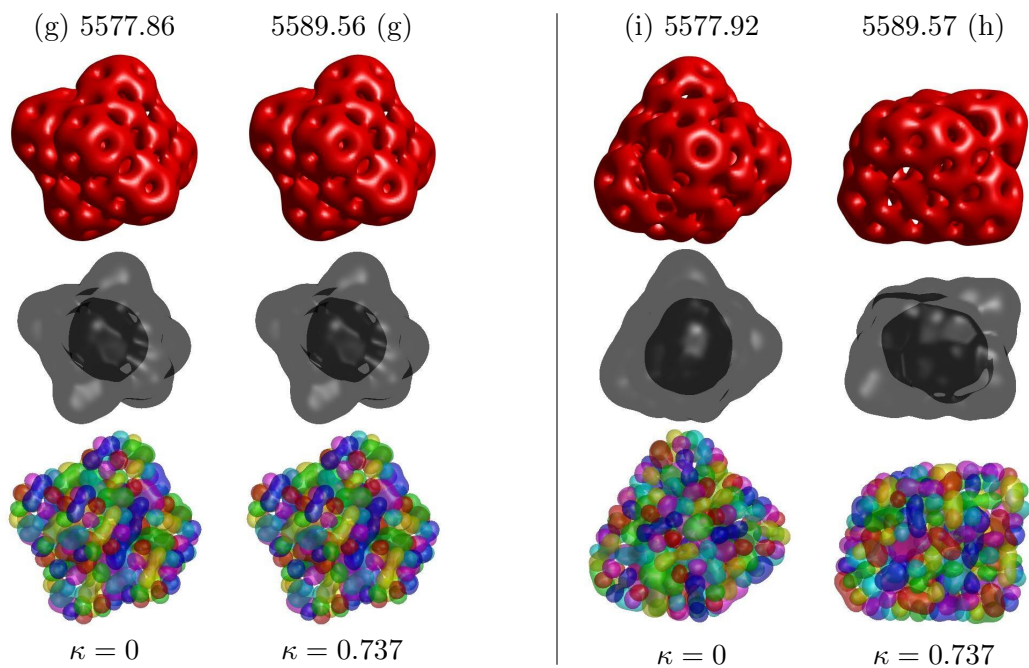


Figure 21: The 7th (left) and 8th (right) lightest $B = 40$ Skyrmions. For details, see the caption of fig. 18.

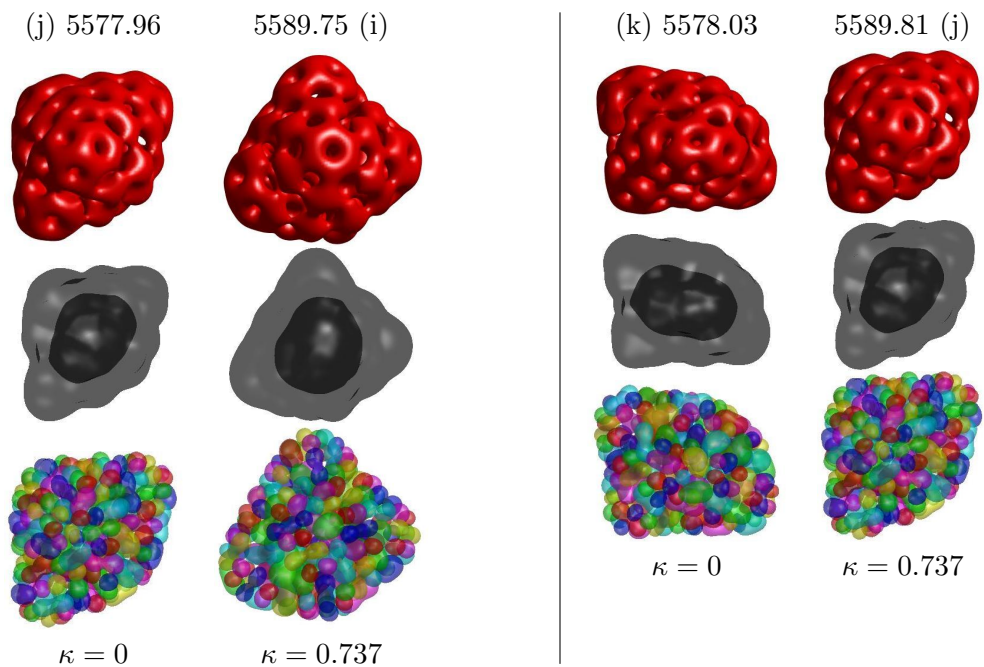


Figure 22: The 9th (left) and 10th (right) lightest $B = 40$ Skyrmions. For details, see the caption of fig. 18.

We start by comparing the ten lightest $B = 40$ Skyrmion solutions in our calibration, with and without the CBR taken into account. The figs. 18-22 show the n -th lightest solution ($n = 1, \dots, 10$) with the CBR turned off on the left-hand side and taken into account on the right-hand side. The three rows correspond to the baryon-charge isosurface, the $\phi_0 = 0$ or $\sigma = 0$ isosurface which is the midpoint between the vacuum and the anti-vacuum, and finally the pion clouds at $\phi_{1,2,3} = 3/4$ shown by red, green and blue and $\phi_{1,2,3} = -3/4$ shown by the corresponding anti-colours. Although all found solutions have been tested to exist both with and without CBR taken into account, it is a quite nice result that for such large Skyrmions as $B = 40$ like the calcium nucleus, the ordering of the lowest-energy states differ when CBR is taken into account or not. We expected this on physical grounds, since it is the largest stable isospin-0 ground state with $B = 4n$ and hence for baryon numbers higher than 40, we expect that the amount of protons is too large to give rise to a stable ground state and hence the isospin must be nonvanishing (yielding more neutrons than protons). The only reason for the number of neutrons and the number of protons being the same, is due to a fact of the strong interactions, i.e. the symmetry energy favours the isospin-0 states, whereas the Coulomb force obviously prefers more neutrons. Clearly a lot of the same solutions appear among the ten lightest $B = 40$ Skyrmions. The two lightest states switch their order when the CBR is turned on, see fig. 18. The 3rd lightest state is the same with and without CBR, see fig. 19(left). The 4th lightest state only appears in top-10 with Coulomb interactions turned on, see fig. 19. Apart from that, the order is the same – with eliminating the flat 40_d -Skyrmion from the CBR-off list, until the 7th-lightest state: This happens to be the same with and without CBR, see fig. 21. Essentially the 40_g -Skyrmion and the 40_h -Skyrmion switch order when the CBR switched off. We also note that with the exception of the 40_d (the 4th lightest solution), all the lightest Skyrmion solutions have a hollow ϕ_0 structure: They basically have a “hole” or a less dense region inside the nucleus that is covered by a shell. It is completely different from the fullerene-type solutions of refs. [44–47] since the “hole” is not the anti-vacuum ($\phi_0 = -1$), but approximately the true vacuum ($\phi_0 = 1$), see figs. 18-22. The fourth-lightest $B = 40$ Skyrmion (40_d) is different, as it is planar in the sense of being of the “graphene”-type solution, see ref. [34].

We will now discuss a few selected Skyrmion configurations that differ from each other when CBR is taken into account or not. First in fig. 23 are shown two cases where the initial configuration (not shown) flows to two different solutions. Taking the two end results, the $\kappa = 0$ solution only changes slightly by taking into account CBR, but the $\kappa = 0.737$ solution disappears when switching off Coulomb interactions.

Another interesting case is shown in fig. 24, where the configuration flows to two different solution depending on whether CBR is taken into account or not. Interestingly, taking the $\kappa = 0$ solution and turning on the Coulomb interaction, the solution flows to the *same* $\kappa = 0.737$ solution as it flowed to from the initial condition. Turning off the Coulomb interaction, however, just yields a slightly deformed version of the $\kappa = 0.737$ solution.

Another odd case is shown in fig. 25, where the solution does not exist when CBR is turned off during the flow from the initial configuration. Turning off the Coulomb

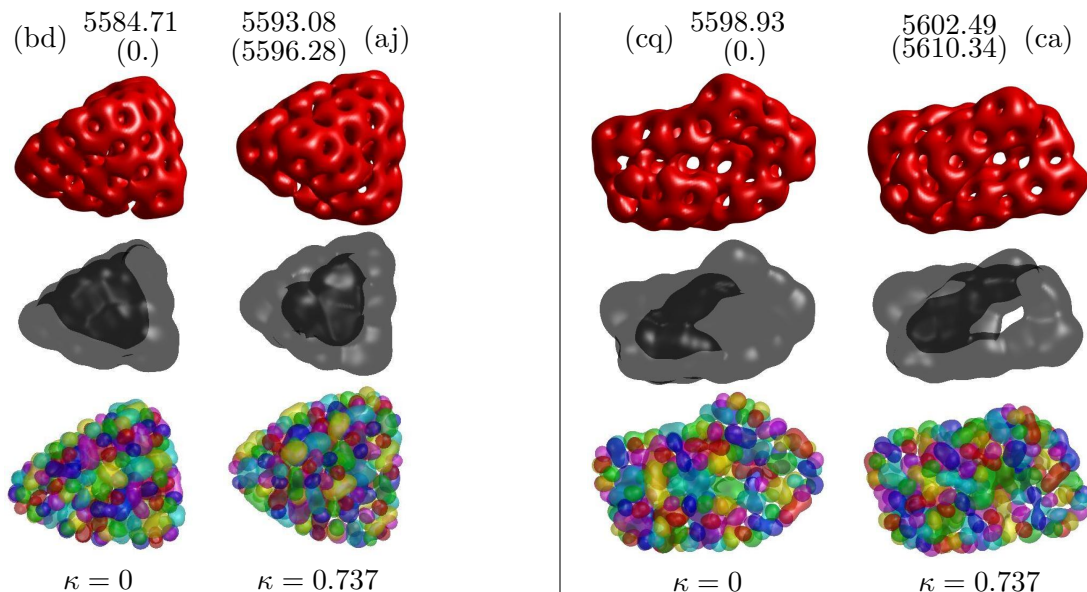


Figure 23: Two cases of a $B = 40$ Skyrmion that flows from an initial condition to two different solutions with and without CBR: Turning on the Coulomb effect on the $\kappa = 0$ solution changes it only slightly (it looks like the $\kappa = 0$ figure and its energy is written in the $\kappa = 0.737$ column in parentheses). Turning off the CBR on the $\kappa = 0.737$ solution, however yields no stable $B = 40$ Skyrmion, in both cases. For details, see the caption of fig. 18.

interaction, however, yields a somewhat deformed version of the $\kappa = 0.737$ solution.

Again a situation that only yields a $B = 40$ solution from a certain initial condition when CBR is taken into account, is shown in fig. 26. In this case, the solution does not change when the Coulomb interaction is turned off (but the total energy decreases slightly, of course, which is shown in parenthesis in the figure).

The final three odd cases are shown in fig. 27; again the solution only exists when CBR is taken into account and more interestingly, taking these final solutions as inputs and switching off the Coulomb interaction gives no stable solution with baryon number $B = 40$.

For completeness, we show the remaining 79 $B = 40$ solutions with higher energies in appendix B.

2.8 The Coulomb energy and the effect of its backreaction

We are finally in a position to summarize the Coulomb energy for a broad range of Skyrmons with baryon numbers 4, 8, 12, 16 and 40 as well as study the detailed effects of the backreaction of the Coulomb force onto the Skyrmons. We begin with the latter.

Figs. 28 through 32 show the (a) baryon charge density, (b) Coulomb (electric) potential, (c) [(d)] difference between the baryon charge density [energy density] with backre-

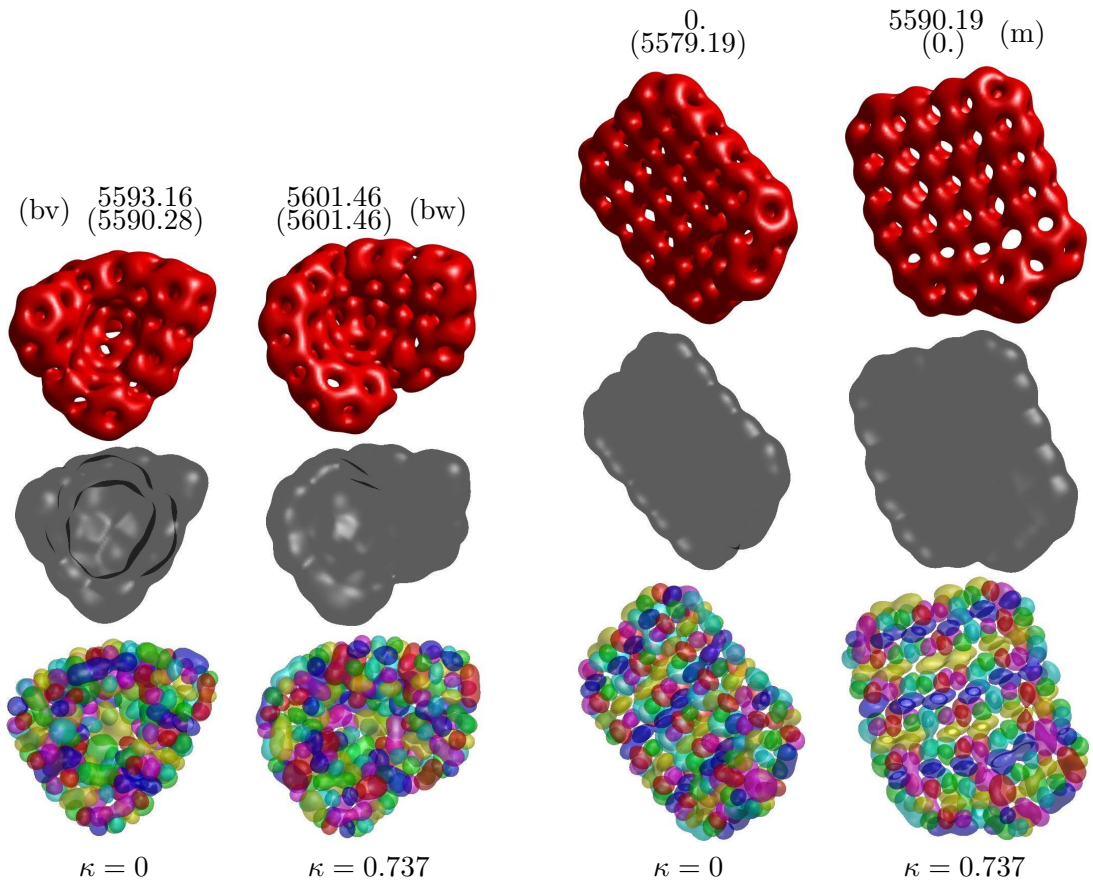


Figure 24: A $B = 40$ Skyrmion that flows from an initial condition to two different solutions with and without CBR: Interestingly, turning on the Coulomb effect on the $\kappa = 0$ solution flows it to the same solution as the initial solution flowed to. Turning off the Coulomb force also does not change the $\kappa = 0.737$ solution.

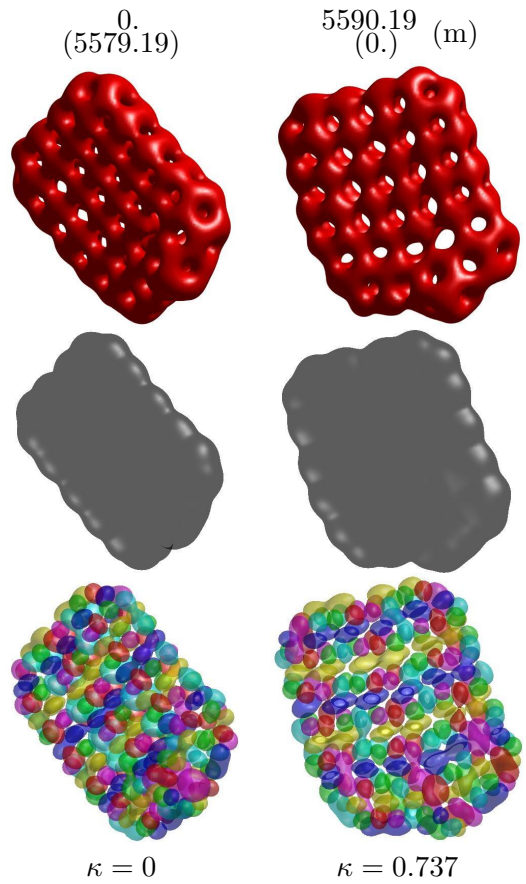


Figure 25: A $B = 40$ Skyrmion that only flows to a $B = 40$ solution with the Coulomb effect turned on. However, switching it off flows this solution to a slightly different solution (shown on the left). For details, see the caption of fig. 18.

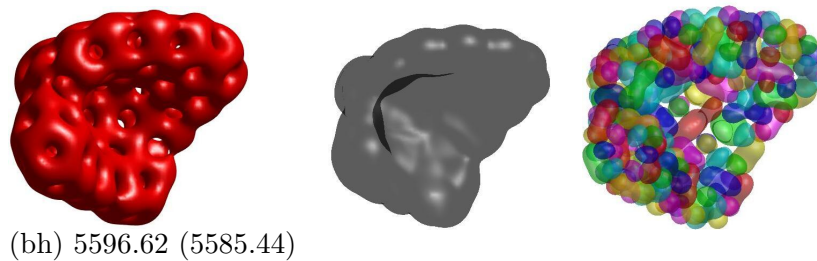


Figure 26: A $B = 40$ Skyrmion that only flows to a solution with the Coulomb effect turned on. Switching off the Coulomb effect, however, yields the same solution (energy shown in parentheses). For details, see the caption of fig. 18.

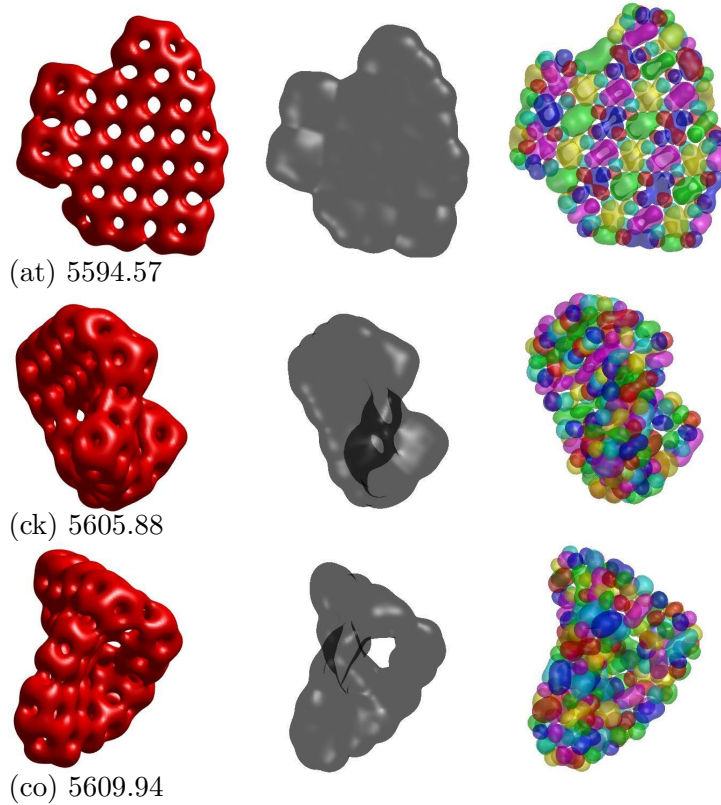


Figure 27: $B = 40$ Skyrmions that only flow to a solution with the Coulomb effect turned on. Switching off the Coulomb effect also yields no solution with $B = 40$. For details, see the caption of fig. 18.

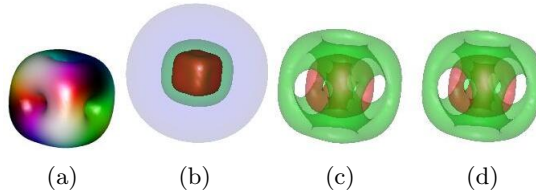


Figure 28: The only $B = 4$ Skyrmion, corresponding to Helium-4: (a) displays the baryon charge isosurface at 1/4 of its maximum density and (b) the Coulomb potential V at 98% (red), 90% (green) and 50% (purple) of its maximum density. The last two panels show the Skyrmion (c) baryon charge density and (d) energy density for the backreacted solution with the non-backreacted solution subtracted off. The green isosurface is showing the positive region at half-maximum density and the red shows the negative region at half-maximum (negative) density. The fact that these differences are positive at larger radii negative at smaller radii means that the backreacted Skyrmion solution is *larger* than the non-backreacted one. The levelsets are at (a) 0.074, (c) green 4.8×10^{-5} , (c) red -2.0×10^{-4} , (d) green 6.4×10^{-3} , (d) red -0.034 and the maximum energy density is for comparison 43.9.

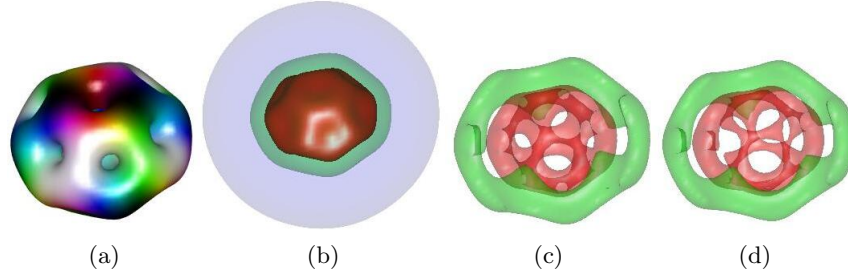


Figure 29: The lightest $B = 8$ Skyrmion in our calibration ($m = 0.65$ and $\kappa = 0.737$), corresponding to Beryllium-8. For details, see the caption of fig. 28. The levelsets are at (a) 0.072, (c) green 1.4×10^{-4} , (c) red -3.6×10^{-4} , (d) green 0.021, (d) red -0.061 and the maximum energy density is for comparison 43.7.

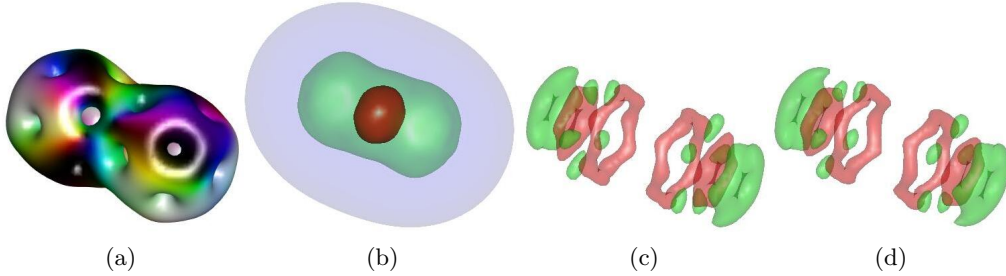


Figure 30: The lightest $B = 12$ Skyrmion in our calibration ($m = 0.65$ and $\kappa = 0.737$), corresponding to Carbon-12. For details, see the caption of fig. 28. The levelsets are at (a) 0.072, (c) green 8.4×10^{-4} , (c) red -1.0×10^{-3} , (d) green 0.12, (d) red -0.16 and the maximum energy density is for comparison 42.6.

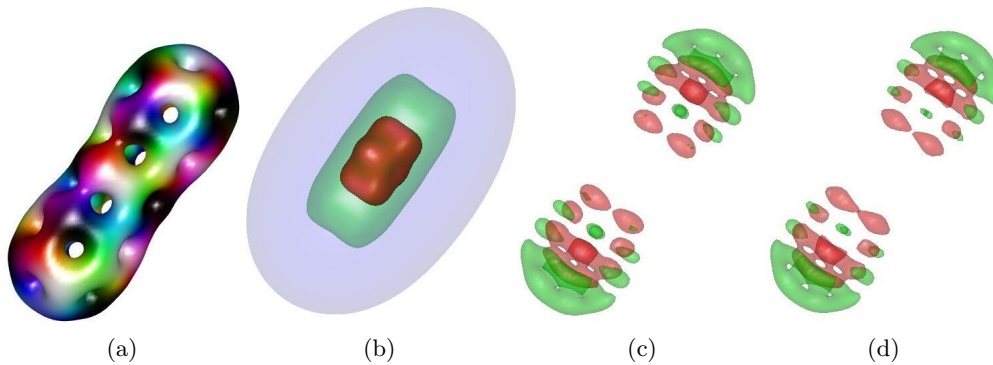


Figure 31: The lightest $B = 16$ Skyrmion in our calibration ($m = 0.65$ and $\kappa = 0.737$), corresponding to Oxygen-16. For details, see the caption of fig. 28. The levelsets are at (a) 0.084, (c) green 6.8×10^{-4} , (c) red -1.0×10^{-3} , (d) green 0.10, (d) red -0.16 and the maximum energy density is for comparison 50.1.

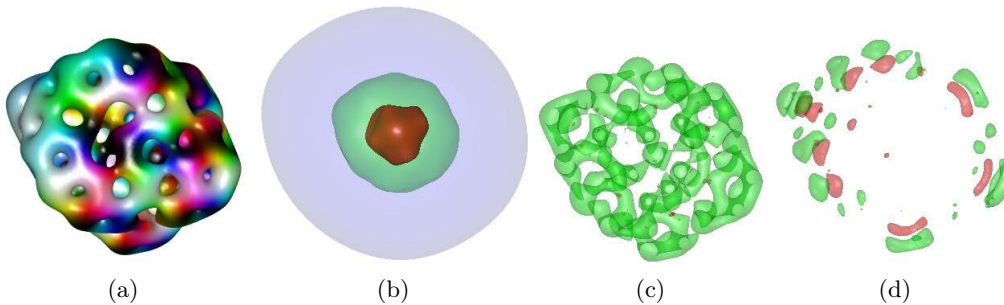


Figure 32: The lightest $B = 40$ Skyrmion in our calibration ($m = 0.65$ and $\kappa = 0.737$), corresponding to Calcium-40. For details, see the caption of fig. 28. The levelsets are at (a) 0.084, (c) green 0.34, (c) red -2.5×10^{-3} , (d) green 0.31, (d) red -0.42 and the maximum energy density is for comparison 50.4.

action of the Coulomb energy and without it. Notice that the red surface (in panel (b)), corresponding to nearly the maximum density of the electric potential (V) has a distinct shape, whereas the half-maximum density (purple) isosurface interpolates between the red surface's shape and a sphere. It is interesting to see in what way the Skyrmons are altered by the backreaction of the Coulomb energy. In the $B = 4$ Skyrmion, the backreaction amounts to increasing the cube isotropically, see fig. 28. This is consistent with the fact that the Coulomb interaction acts similarly to the Skyrme term, but with a much smaller effect due to the smallness of the electromagnetic coupling (charge). For the $B = 8$ Skyrmion, the solution increases not isotropically but more in the direction of the rim, see fig. 29. In the larger $B = 12$ and $B = 16$ Skyrmons, the increase of the Skyrmons' sizes takes place along the axis aligned with the Skyrmion's longest length. Finally, the $B = 40$ Skyrmion also grows, but in this case it seems more complicated than with the simpler Skyrmons.

Table 3 shows the total energies, Coulomb energies and charge radii of the lightest Skyrmion solutions with baryon numbers 4, 8, 12, 16 and 40. Additionally, experimental data is used for comparison from the NuDat3 database [48–52]. The total energies are surprisingly well described by the model in our calibration, with the largest deviation of 1.86% (excess) for Helium-4 and only -0.96% deviation for Calcium-40. The fact that there is an excess in the energies for $B < 12$ and a lack for $B > 12$ illustrates that the Skyrme model is too tightly bound – i.e. the good old story of the too large binding energies. Nevertheless, the problem is much milder than one would anticipate, when looking only at large Skyrmons and ignoring the energy for the single nucleon ($B = 1$). Of course, these energies are classical and no quantum corrections from vibrational modes etc. have been taken into account here (recall that for spin-0 and isospin-0 states, there are no contribution from the zeromode quantization of the Skyrmons).

Even though the total energies are predicted very precisely in our calibration, the Coulomb energies are more imprecise and of the usual order of magnitude of errors in Skyrme-type models. Specifically, the Coulomb energies are consistently overestimated by between 3.3% and 21.9%, with Oxygen-16 being the most precise and Helium-4 the most

	$B = 4$	Helium-4	abs. diff.	rel. diff.
E	575.41			
E	3.797 GeV	3.727 GeV	69.5 MeV	1.86%
E_C	1.919 MeV	1.575 MeV	0.3 MeV	21.87%
R	1.422 fm	1.678 fm	-0.256 fm	-15.24%
	$B = 8$	Beryllium-8	abs. diff.	rel. diff.
E	1133.65			
E	7.481 GeV	7.455 GeV	25.7 MeV	0.34%
E_C	5.713 MeV	5.000 MeV	0.7 MeV	14.26%
R	1.908 fm	-	-	-
	$B = 12$	Carbon-12	abs. diff.	rel. diff.
E	1693.85			
E	11.177 GeV	11.177 GeV	0.0 MeV	0.00%
E_C	10.591 MeV	9.828 MeV	0.8 MeV	7.77%
R	2.471 fm	2.470 fm	0.001 fm	0.04%
	$B = 16$	Oxygen-16	abs. diff.	rel. diff.
E	2250.87			
E	14.853 GeV	14.895 GeV	-42.5 MeV	-0.29%
E_C	16.389 MeV	15.874 MeV	0.5 MeV	3.25%
R	3.002 fm	2.699 fm	0.303 fm	11.23%
	$B = 40$	Calcium-40	abs. diff.	rel. diff.
E	5585.62			
E	36.858 GeV	37.215 GeV	-357.4 MeV	-0.96%
E_C	77.388 MeV	73.100 MeV	4.3 MeV	5.86%
R	3.525 fm	3.478 fm	0.047 fm	1.35%

Table 3: Total energy in Skyrme units, total energy in GeV compared with experimental data [48–52], Coulomb energy in MeV compared with the fit $0.156B^{\frac{5}{3}}$ of ref. [53], and charge radii compared with experimental data [48–52]. The comparison is made both in absolute values and in percentages.

imprecise. The charge radii are slightly better with the Helium-4 being 15.2% too small and Oxygen-16 being 11.2% too large, as the two extremes.

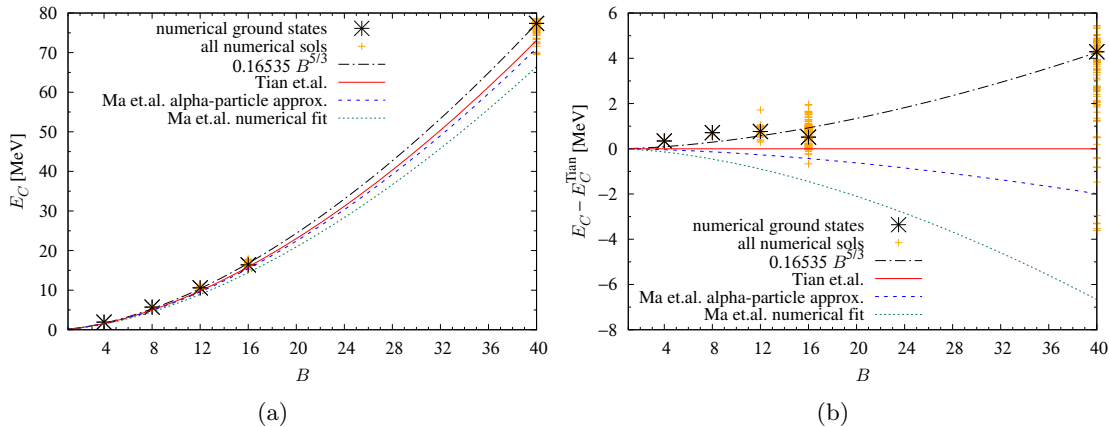


Figure 33: Coulomb energies of the lightest Skyrmions (black crosses) as well as all remaining solutions (orange pluses). The lightest Skyrmions are fitted to the power-law shown with a black dot-dashed line. In comparison, the experimental fit of Tian et.al. [53] and two fits of Ma et.al. [32] are shown. Panel (b) shows the same information, but relative to the fit of Tian et.al. [53].

Compiling the Coulomb energies into a figure, we show in fig. 33 the Coulomb energies computed for the ground states (the global energy minimizers for each baryon number) with a large black cross and all the remaining solutions with smaller orange pluses. Taking as the “experimental” fit, the fitted result of Tian et.al. [53], our ground states are all slightly above the nuclear “experimental” fit, but only about 4 MeV for Calcium-40 and less or about 1 MeV for the other 4 nuclei. We summarize the four different Coulomb fits that are shown in fig. 33:

$$\begin{aligned}
 E_C^{\text{Tian}} &= 0.156B^{\frac{5}{3}} \text{ MeV}, \\
 E_C^{\text{Ma, APA}} &= 0.152B^{\frac{5}{3}} \text{ MeV}, \\
 E_C^{\text{Ma, num}} &= 0.142B^{\frac{5}{3}} \text{ MeV}, \\
 E_C^{\text{fit}} &= 0.165B^{\frac{5}{3}} \text{ MeV},
 \end{aligned} \tag{2.69}$$

with E_C^{Tian} being the simplest fit of ref. [53], $E_C^{\text{Ma, APA}}$ being the fit to the alpha-particle approximation of ref. [32], $E_C^{\text{Ma, num}}$ being a fit to their numerical alpha-particle solutions, and finally E_C^{fit} being a fit to our ground states in our calibration. It is worth mentioning that the fit of ref. [53] is based on nuclei in the range $B \sim 11-75$ and hence is not fitted on our two lightest nuclei ($B = 4$ and $B = 8$). It is perhaps also important to notice that their fit is made on nuclei, not only having vanishing isospin, so a fit in the isospin-0 sector may be more precise than the fit of ref. [53].

3 Conclusion and discussion

In this paper, we have considered the standard Skyrme model with the addition of the Maxwell term and a source term for the electric field that matches with the Gell-Mann-Nishijima relation. Formally, the equations are identical to those of the ω -Skyrme model [35], with the identification of the electric potential A_0 and ω_0 and with the exception that A_0 is massless whereas ω_0 is massive. This gives rise to a technical complication, because A_0 with a power-like falloff requires in principle very large domains for obtaining its solution. We solve this problem with the approximation of assuming that the electric charge is approximately interchangeable with a point charge at the centre-of-mass of the Skyrmion, as seen at the distance of the boundary of the box in which the numerical equations are solved. This would be a poor approximation, if not used in conjunction with the trick of integrating-by-parts, so that the Coulomb energy is evaluated as the product of the electric charge density (Skyrmion baryon charge density) and the electric potential, integrated over space. Since the Skyrmion baryon charge density is exponentially spatially localized in the massive Skyrme model, so is this product. We calibrate the model to the size and energy of Carbon-12, which is a relatively large nucleus, thus giving a larger range of “good behaviour” of our fit in baryon numbers. The fit, however, requires a pion mass parameter smaller than unity (often used in the literature) and this fact changes the solutions and ground states (lightest Skyrmion solutions) with respect to the Smörgåsbord of ref. [34]. We find that the “dynamics” of the Skyrmons is more sensitive to the inclusion of the Coulomb backreaction (CBR) than the final state outcome. That is, starting with a particular initial condition, turning CBR on or off may very likely result in different (local) solutions, whereas the global minimizer of the energy is often the same. It turns out that for the largest stable nucleus with baryon number $B = 4n$ and isospin zero in the ground state, Calcium-40, the lightest Skyrmion solutions differ with the CBR turned on or off. We fit the Coulomb energies of our Skyrmons and find that the coefficient of the power-law is larger than the phenomenological one of ref. [53], which in turn is larger than the result of ref. [32]. Nevertheless, the Coulomb energies are within about 15% of the phenomenological fits, which is quite reasonable for a simple over-bound Skyrme model without quantization taken into account. We notice that the total energies are remarkably well described by our solutions in our calibration, with the largest deviation of 1.86%. Finally, we should point out that the 100 $B = 40$ solutions are new and due to the complexity of such large Skyrmons, we cannot for sure say that we have found the global minimizer of the energy.

Clearly, the Coulomb effect is important for large nuclei and taking it into account with a source term is just the simplest approach. As explained in detail in the introduction, there is a more elaborate approach of gauging the Skyrme model and including Wess-Zumino-like or Callan-Witten terms that reproduce the QCD anomalies. Such an approach would complicate the model significantly and the fact that the Coulomb effect is most pronounced for large nuclei, requires one to study large Skyrmons, like the $B = 40$ Skyrmons studied in this paper.

Acknowledgements

S. B. G. thanks the Outstanding Talent Program of Henan University and the Ministry of Education of Henan Province for partial support. The work of S. B. G. is supported by the National Natural Science Foundation of China (Grant No. 12071111) and by the Ministry of Science and Technology of China (Grant No. G2022026021L).

References

- [1] S. Scherer, *Introduction to chiral perturbation theory*, *Adv. Nucl. Phys.* **27** (2003) 277, [[hep-ph/0210398](#)].
- [2] T. H. R. Skyrme, *A Nonlinear field theory*, *Proc. Roy. Soc. Lond. A* **260** (1961) 127–138.
- [3] T. H. R. Skyrme, *A Unified Field Theory of Mesons and Baryons*, *Nucl. Phys.* **31** (1962) 556–569.
- [4] K. Krasnov, *Gravity as a diffeomorphism invariant gauge theory*, *Phys. Rev. D* **84** (2011) 024034, [[arXiv:1101.4788](#)].
- [5] A. Pais, *Remark on baryon conservation*, *Phys. Rev. D* **8** (1973) 1844–1846.
- [6] C. G. Callan, Jr. and E. Witten, *Monopole Catalysis of Skyrmion Decay*, *Nucl. Phys. B* **239** (1984) 161–176.
- [7] B. M. A. G. Piette and D. H. Tchrakian, *Static solutions in the $U(1)$ gauged Skyrme model*, *Phys. Rev. D* **62** (2000) 025020, [[hep-th/9709189](#)].
- [8] F. Navarro-Lerida, E. Radu, and D. H. Tchrakian, *The role of the Callan–Witten anomaly density as a Chern–Simons term in Skyrme model **, *J. Phys. A* **56** (2023), no. 46 465401, [[arXiv:2304.12648](#)].
- [9] E. Radu and D. H. Tchrakian, *Spinning $U(1)$ gauged skyrmions*, *Phys. Lett. B* **632** (2006) 109–113, [[hep-th/0509014](#)].
- [10] L. R. Livramento, E. Radu, and Y. Shnir, *Solitons in the Gauged Skyrme-Maxwell Model*, *SIGMA* **19** (2023) 042, [[arXiv:2301.12848](#)].
- [11] L. R. Livramento and Y. Shnir, *Multisolitons in a gauged Skyrme-Maxwell model*, *Phys. Rev. D* **108** (2023), no. 6 065010, [[arXiv:2307.05756](#)].
- [12] R. Kirichenkov, J. Kunz, N. Sawado, and Y. Shnir, *Skyrmions and pion stars in the gauged $U(1)$ Einstein-Skyrme model*, *Phys. Rev. D* **109** (2024), no. 4 045002, [[arXiv:2311.12432](#)].
- [13] J. Cork, D. Harland, and T. Winyard, *A model for gauged skyrmions with low binding energies*, *J. Phys. A* **55** (2022), no. 1 015204, [[arXiv:2109.06886](#)].
- [14] J. Cork and D. Harland, *Geometry of Gauged Skyrmions*, *SIGMA* **19** (2023) 071, [[arXiv:2303.02623](#)].
- [15] S. B. Gudnason and C. Halcrow, *Quantum binding energies in the Skyrme model*, *Phys. Lett. B* **850** (2024) 138526, [[arXiv:2307.09272](#)].
- [16] M. Ohtani and K. Ohta, *Skyrmions coupled with the electromagnetic field via the gauged Wess-Zumino term*, *Phys. Rev. D* **70** (2004) 096014, [[hep-ph/0406173](#)].
- [17] M. Ohtani and K. Ohta, *Spin polarized Skyrmions in the $U(EM)(1)$ gauged Wess-Zumino action*, *Nucl. Phys. A* **755** (2005) 661–664.

- [18] B.-R. He, *Skyrme model study of proton and neutron properties in a strong magnetic field*, *Phys. Lett. B* **765** (2017) 109–112, [[arXiv:1609.09055](#)].
- [19] L. Avilés, F. Canfora, N. Dimakis, and D. Hidalgo, *Analytic topologically nontrivial solutions of the (3+1)-dimensional U(1) gauged Skyrme model and extended duality*, *Phys. Rev. D* **96** (2017), no. 12 125005, [[arXiv:1711.07408](#)].
- [20] F. Canfora, M. Lagos, S. H. Oh, J. Oliva, and A. Vera, *Analytic (3+1)-dimensional gauged Skyrmions, Heun, and Whittaker-Hill equations and resurgence*, *Phys. Rev. D* **98** (2018), no. 8 085003, [[arXiv:1809.10386](#)].
- [21] F. Canfora, N. Dimakis, and A. Paliathanasis, *Analytic Studies of Static and Transport Properties of (Gauged) Skyrmions*, *Eur. Phys. J. C* **79** (2019), no. 2 139, [[arXiv:1902.01563](#)].
- [22] T. Sakai and S. Sugimoto, *Low energy hadron physics in holographic QCD*, *Prog. Theor. Phys.* **113** (2005) 843–882, [[hep-th/0412141](#)].
- [23] A. Rebhan, *The Witten-Sakai-Sugimoto model: A brief review and some recent results*, *EPJ Web Conf.* **95** (2015) 02005, [[arXiv:1410.8858](#)].
- [24] M. F. Atiyah and N. S. Manton, *Skyrmions From Instantons*, *Phys. Lett. B* **222** (1989) 438–442.
- [25] S. Bolognesi and P. Sutcliffe, *The Sakai-Sugimoto soliton*, *JHEP* **01** (2014) 078, [[arXiv:1309.1396](#)].
- [26] E. Witten, *Anti-de Sitter space and holography*, *Adv. Theor. Math. Phys.* **2** (1998) 253–291, [[hep-th/9802150](#)].
- [27] C. V. Johnson and A. Kundu, *External Fields and Chiral Symmetry Breaking in the Sakai-Sugimoto Model*, *JHEP* **12** (2008) 053, [[arXiv:0803.0038](#)].
- [28] O. Bergman, G. Lifschytz, and M. Lippert, *Response of Holographic QCD to Electric and Magnetic Fields*, *JHEP* **05** (2008) 007, [[arXiv:0802.3720](#)].
- [29] E. Bonenfant, L. Harbour, and L. Marleau, *Near-BPS Skyrmions: Non-shell configurations and Coulomb effects*, *Phys. Rev. D* **85** (2012) 114045, [[arXiv:1205.1414](#)].
- [30] C. Adam, C. Naya, J. Sanchez-Guillen, and A. Wereszczynski, *Nuclear binding energies from a Bogomol’nyi-Prasad-Sommerfield Skyrme model*, *Phys. Rev. C* **88** (2013), no. 5 054313, [[arXiv:1309.0820](#)].
- [31] C. Adam, C. Naya, J. Sanchez-Guillen, and A. Wereszczynski, *Bogomol’nyi-Prasad-Sommerfield Skyrme Model and Nuclear Binding Energies*, *Phys. Rev. Lett.* **111** (2013), no. 23 232501, [[arXiv:1312.2960](#)].
- [32] N. Ma, C. J. Halcrow, and H. Zhang, *Effect of the Coulomb energy on Skyrmions*, *Phys. Rev. C* **99** (2019), no. 4 044312, [[arXiv:1901.06025](#)].
- [33] B. C. Carlson and G. L. Morley, *Multipole Expansion of Coulomb Energy*, *American Journal of Physics* **31** (03, 1963) 209–211, [https://pubs.aip.org/aapt/ajp/article-pdf/31/3/209/10110064/209_1_online.pdf].
- [34] S. B. Gudnason and C. Halcrow, *A Smörgåsbord of Skyrmions*, *JHEP* **08** (2022) 117, [[arXiv:2202.01792](#)].
- [35] S. B. Gudnason and J. M. Speight, *Realistic classical binding energies in the ω -Skyrme model*, *JHEP* **07** (2020) 184, [[arXiv:2004.12862](#)].

- [36] N. S. Manton and P. Sutcliffe, *Topological solitons*. Cambridge Monographs on Mathematical Physics. Cambridge University Press, 2004.
- [37] G. H. Derrick, *Comments on nonlinear wave equations as models for elementary particles*, *J. Math. Phys.* **5** (1964) 1252–1254.
- [38] D. Harland, *Topological energy bounds for the Skyrme and Faddeev models with massive pions*, *Phys. Lett. B* **728** (2014) 518–523, [[arXiv:1311.2403](#)].
- [39] C. Adam and A. Wereszczynski, *Topological energy bounds in generalized Skyrme models*, *Phys. Rev. D* **89** (2014), no. 6 065010, [[arXiv:1311.2939](#)].
- [40] **Particle Data Group** Collaboration, P. A. Zyla et al., *Review of Particle Physics*, *PTEP* **2020** (2020), no. 8 083C01.
- [41] I. Angeli and K. P. Marinova, *Table of experimental nuclear ground state charge radii: An update*, *Atom. Data Nucl. Data Tabl.* **99** (2013), no. 1 69–95.
- [42] G. S. Adkins, C. R. Nappi, and E. Witten, *Static Properties of Nucleons in the Skyrme Model*, *Nucl. Phys. B* **228** (1983) 552.
- [43] N. S. Manton and S. W. Wood, *Reparametrising the Skyrme model using the lithium-6 nucleus*, *Phys. Rev. D* **74** (2006) 125017, [[hep-th/0609185](#)].
- [44] R. A. Battye and P. M. Sutcliffe, *Symmetric skyrmions*, *Phys. Rev. Lett.* **79** (1997) 363–366, [[hep-th/9702089](#)].
- [45] C. J. Houghton, N. S. Manton, and P. M. Sutcliffe, *Rational maps, monopoles and Skyrmions*, *Nucl. Phys. B* **510** (1998) 507–537, [[hep-th/9705151](#)].
- [46] R. M. Battye and P. M. Sutcliffe, *Solitonic fullerenes*, *Phys. Rev. Lett.* **86** (2001) 3989–3992, [[hep-th/0012215](#)].
- [47] R. A. Battye and P. M. Sutcliffe, *Skyrmions, fullerenes and rational maps*, *Rev. Math. Phys.* **14** (2002) 29–86, [[hep-th/0103026](#)].
- [48] “Nudat3 database – helium-4.” Accessed on September 26, 2024.
- [49] “Nudat3 database – beryllium-8.” Accessed on September 26, 2024.
- [50] “Nudat3 database – carbon-12.” Accessed on September 26, 2024.
- [51] “Nudat3 database – oxygen-16.” Accessed on September 26, 2024.
- [52] “Nudat3 database – calcium-40.” Accessed on September 26, 2024.
- [53] J. Tian, H. Cui, N. Wang, and K. Zheng, *Effect of Coulomb energy on the symmetry energy coefficients of finite nuclei*, *Phys. Rev. C* **90** (2014), no. 2 024313, [[arXiv:1403.6560](#)].

Appendices

A Proof of Lemma 1

Let $\rho : \mathbb{R}^3 \rightarrow \mathbb{R}$ satisfy $|\rho(x)| \leq Ce^{-|x|/C}$ and $V : \mathbb{R}^3 \rightarrow \mathbb{R}$ be the electrostatic potential it induces, that is, the unique solution of (2.29) decaying at infinity. Then

$$V(x) = \frac{1}{4\pi\epsilon_0} \int_{\mathbb{R}^3} \frac{\rho(x')}{|x-x'|} d^3x', \quad (\text{A.1})$$

and it follows immediately that $|V(x)| \leq C^3 V_*(x/C)$, where V_* is the potential induced by $\rho_*(x) = e^{-|x|}$. The electric field $E_* = -\nabla V_*$ induced by ρ_* is radial, so we may compute V_* explicitly by an application of the divergence theorem, obtaining

$$V_*(x) = \frac{1}{\varepsilon_0} \left[\frac{2}{r} - e^{-r} \left(1 + \frac{2}{r} \right) \right], \quad (\text{A.2})$$

and the claimed localization of V immediately follows.

Let $E = -\nabla V$ be the electric field induced by ρ . We seek an upper bound on $|n \cdot E|$ where $n = x/r$ is the unit radial vector. Now (A.1) implies that

$$E = \frac{1}{4\pi\varepsilon_0} \int_{\mathbb{R}^3} \frac{x - x'}{|x - x'|^3} \rho(x') d^3 x', \quad (\text{A.3})$$

and hence that

$$|n \cdot E| \leq \frac{1}{4\pi\varepsilon_0} \int_{\mathbb{R}^3} \frac{|\rho(x')|}{|x - x'|^2} d^3 x' \quad (\text{A.4})$$

$$\leq \frac{C}{4\pi\varepsilon_0} \int_{\mathbb{R}^3} \frac{e^{-|x'|/C}}{|x - x'|^2} d^3 x' = \frac{C}{4\pi\varepsilon_0} f(r) \quad (\text{A.5})$$

where

$$\begin{aligned} f(r) &= 2\pi \int_{-1}^1 dz \int_0^\infty ds \frac{s^2 e^{-s/C}}{s^2 + r^2 - 2zsr} \\ &= 2\pi \int_0^\infty ds s e^{-s/C} \log \left| \frac{s+r}{s-r} \right| \\ &= 2\pi r \int_0^\infty ds s e^{-(r/C)s} \log \left| \frac{s+1}{s-1} \right| \end{aligned} \quad (\text{A.6})$$

Choose and fix $\varepsilon \in (0, 1/2)$. Then there exists $K > 0$ such that

$$\log \left| \frac{s+1}{s-1} \right| \leq \begin{cases} Ks, & s \in [0, 1 - \varepsilon], \\ K \log \left(\frac{1}{1-s} \right), & s \in [1 - \varepsilon, 1), \\ K \log \left(\frac{1}{s-1} \right), & s \in (1, 1 + \varepsilon], \\ K/s, & s \in [1 + \varepsilon, \infty). \end{cases} \quad (\text{A.7})$$

Hence

$$\begin{aligned} f(r) &\leq 2\pi r K \left\{ 2 \left(\frac{C}{r} \right)^3 + \frac{e^{-r/C}}{r/C} + \varepsilon(1 - \log \varepsilon) e^{-(r/C)(1-\varepsilon)} + \varepsilon(1 - \log \varepsilon)(1 + \varepsilon) e^{-r/C} \right\} \\ &\leq \frac{K'}{r^2} \end{aligned} \quad (\text{A.8})$$

for some $K' > 0$. The claimed localization of $|\partial V / \partial r| = |n \cdot E|$ now follows.

B The remaining $B = 40$ solutions

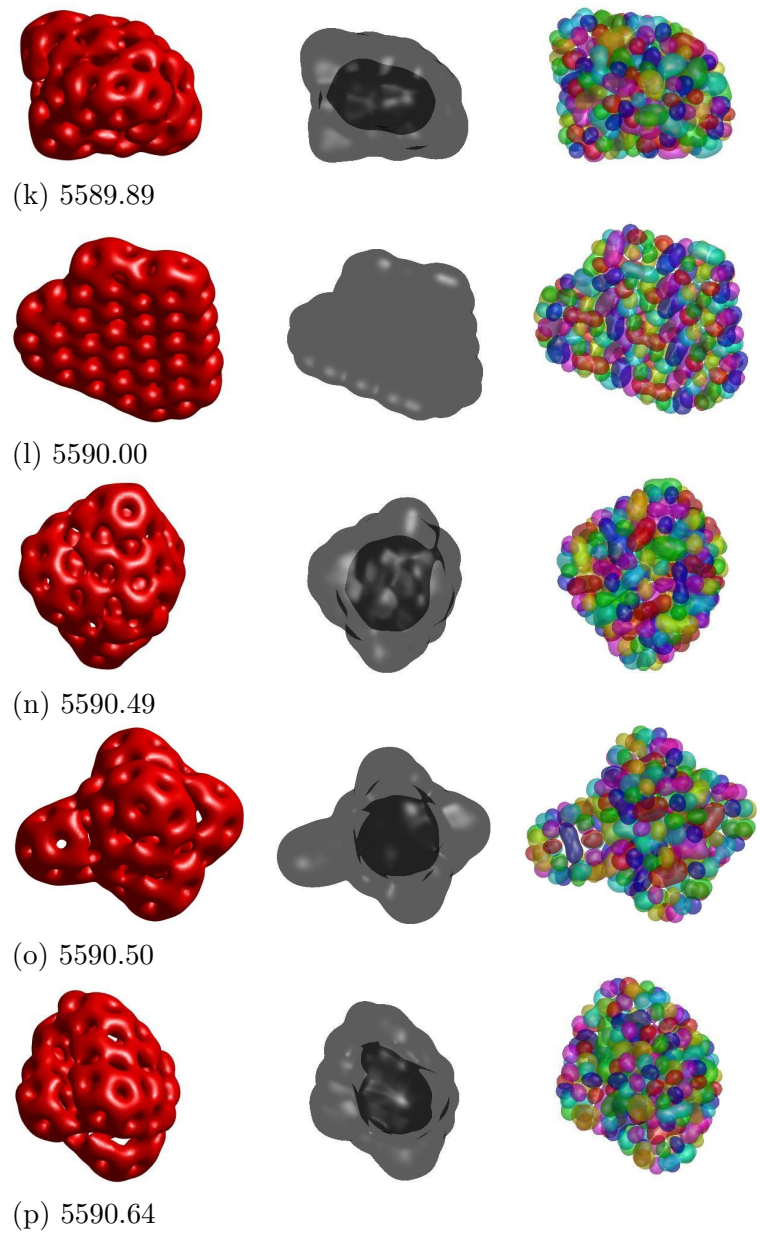


Figure 34: $B = 40$ solutions with $\kappa = 0.737$ ordered by increasing static energy, excluding the 10 lightest solutions as well as that of fig. 25.

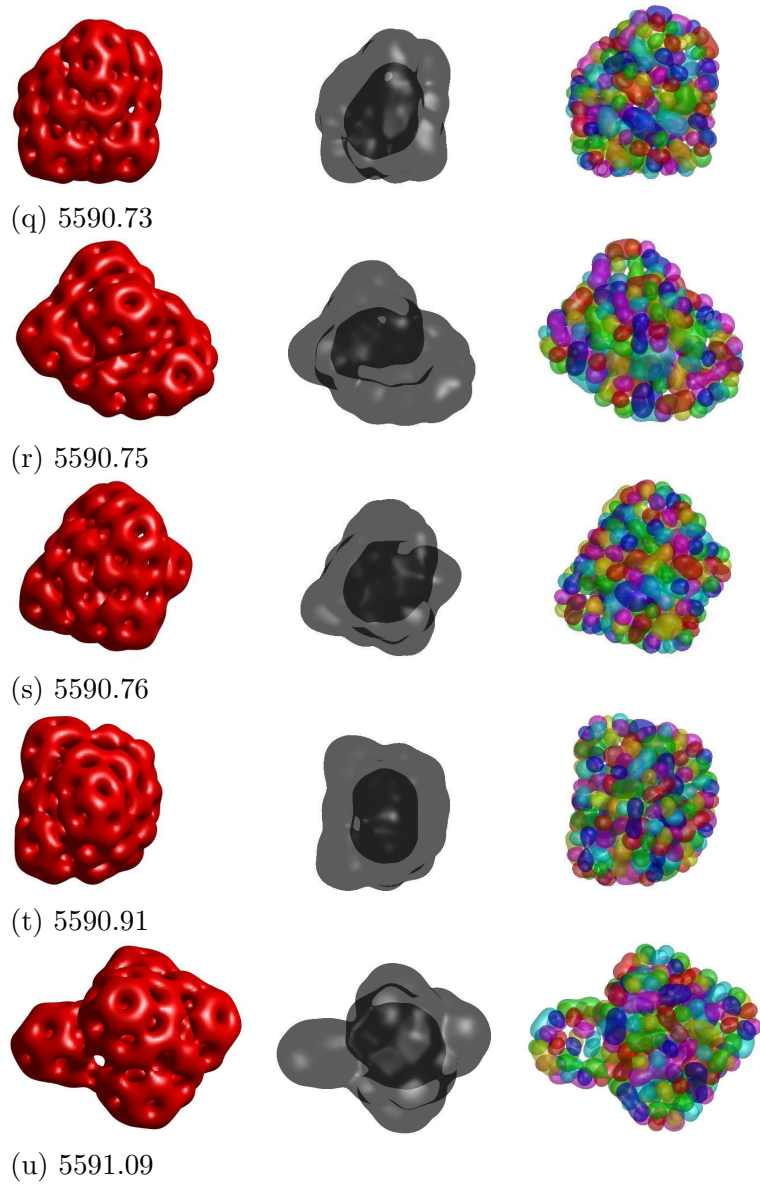


Figure 35: $B = 40$ solutions with $\kappa = 0.737$ ordered by increasing static energy, continued from fig. 34.

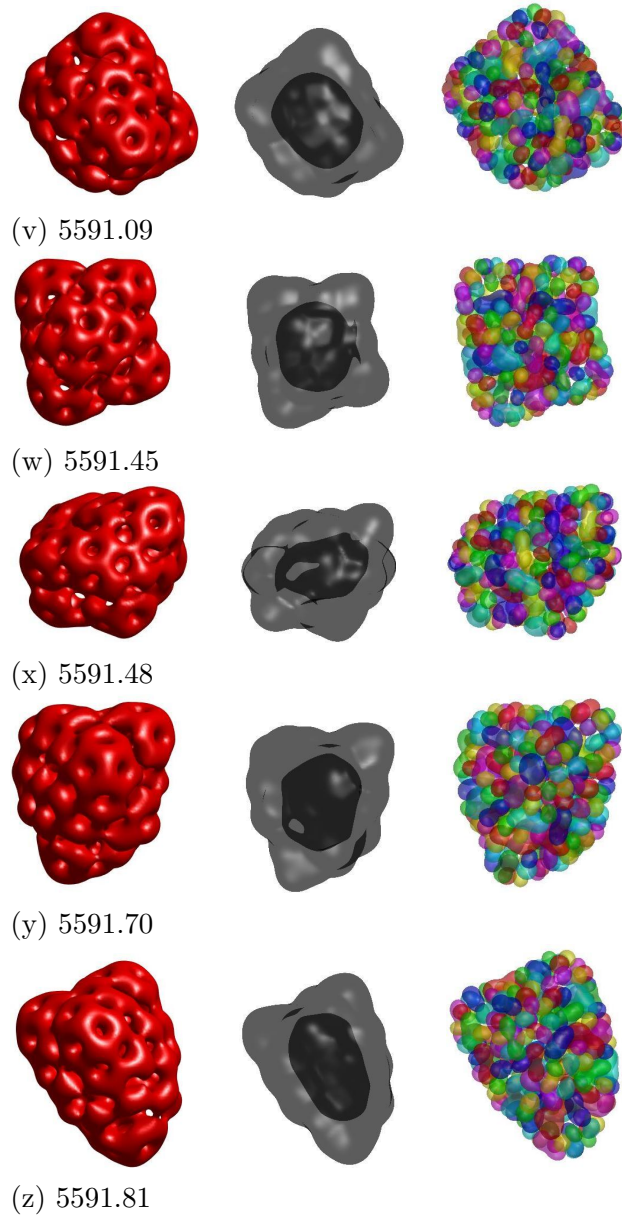


Figure 36: $B = 40$ solutions with $\kappa = 0.737$ ordered by increasing static energy, continued from fig. 35.

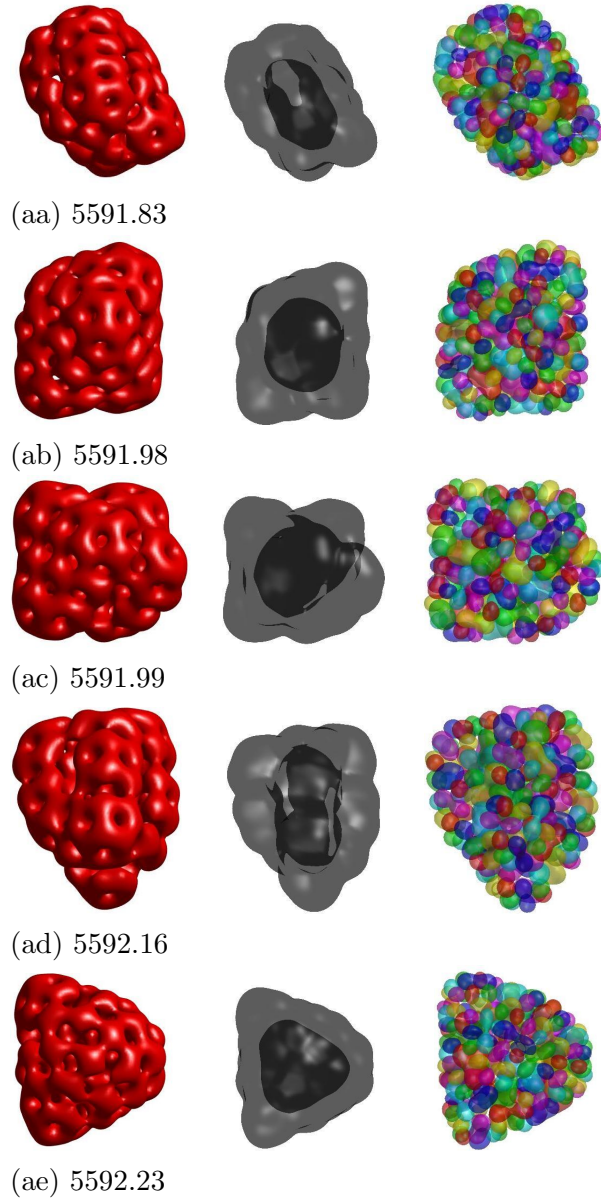


Figure 37: $B = 40$ solutions with $\kappa = 0.737$ ordered by increasing static energy, continued from fig. 36.

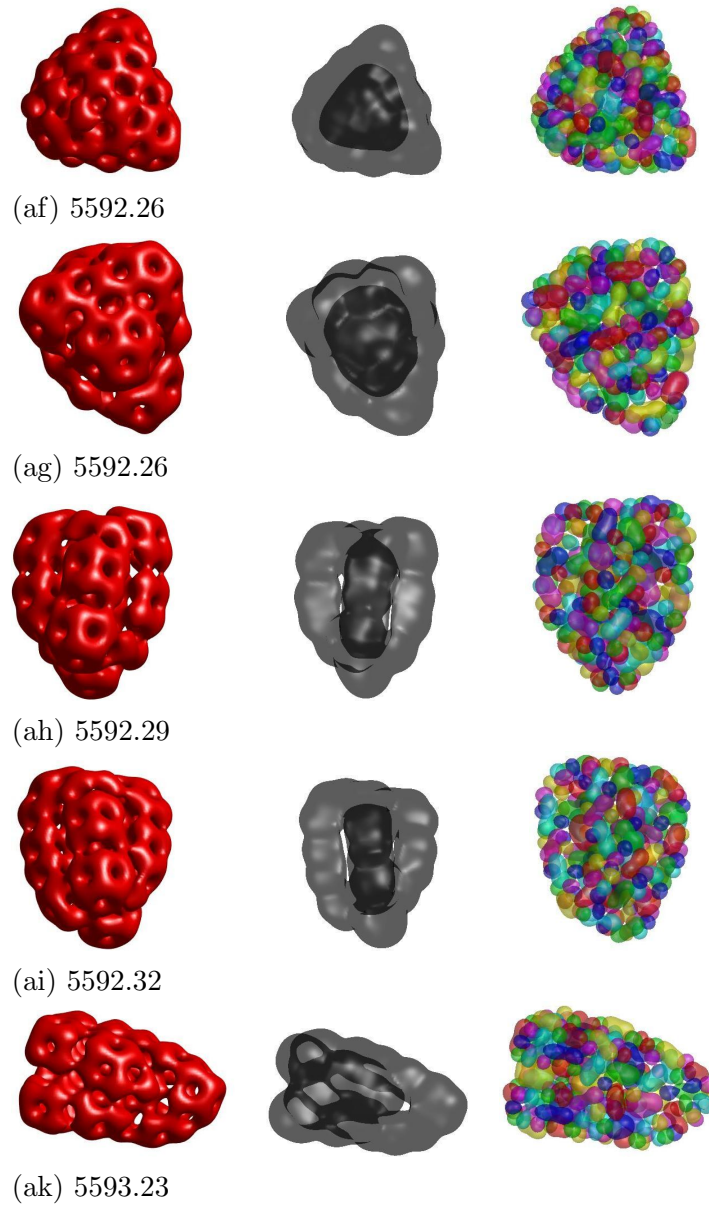


Figure 38: $B = 40$ solutions with $\kappa = 0.737$ ordered by increasing static energy, continued from fig. 37 and excluding that of fig. 23(left).

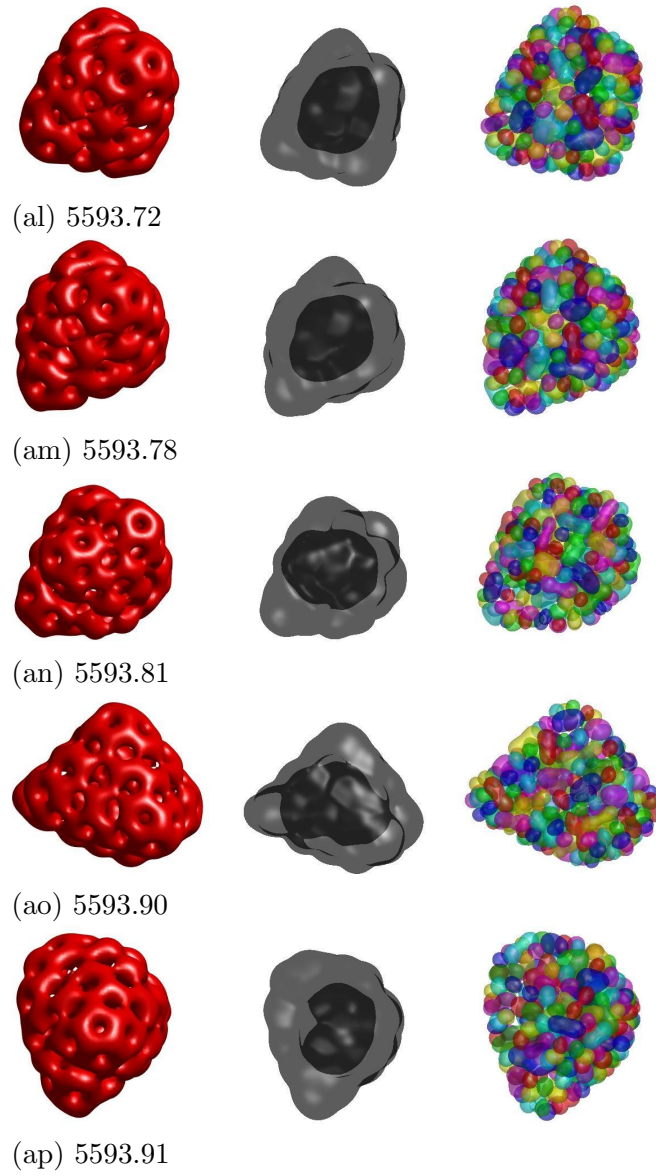


Figure 39: $B = 40$ solutions with $\kappa = 0.737$ ordered by increasing static energy, continued from fig. 38.

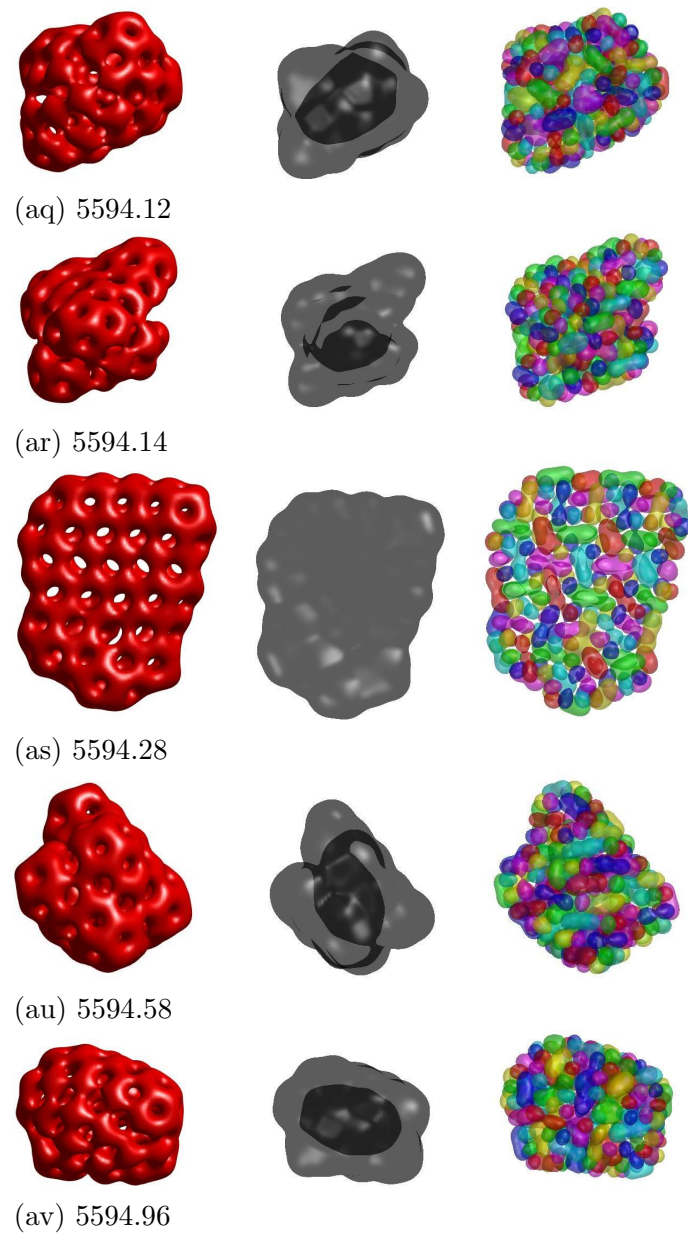


Figure 40: $B = 40$ solutions with $\kappa = 0.737$ ordered by increasing static energy, continued from fig. 39 and excluding the second row of fig. 27.

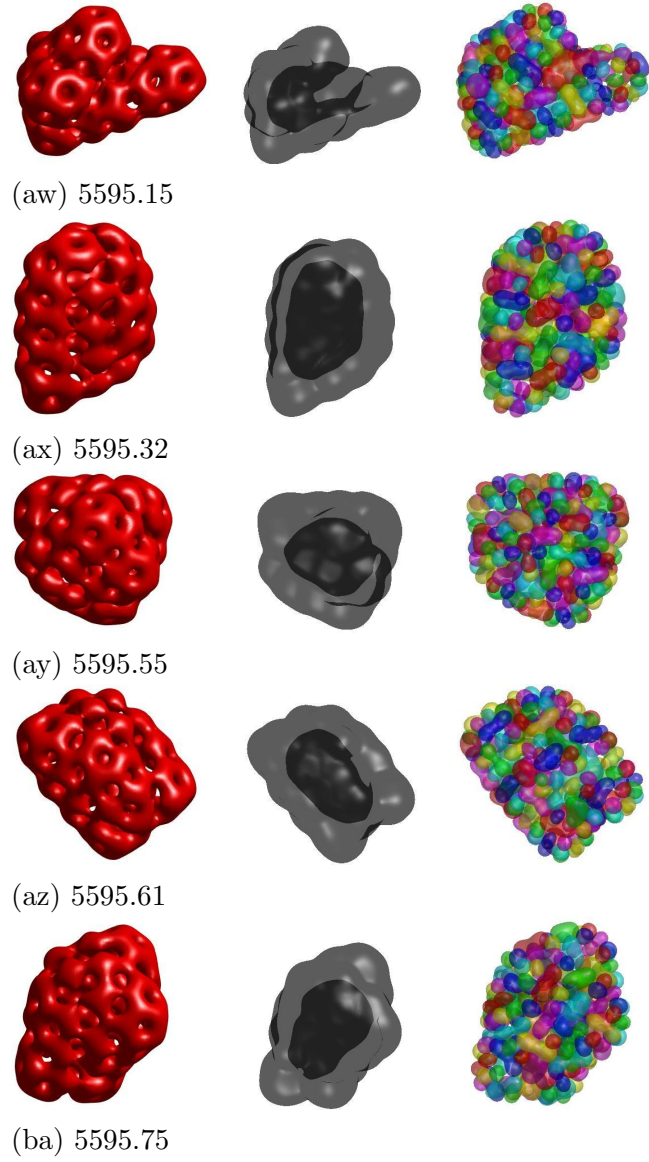


Figure 41: $B = 40$ solutions with $\kappa = 0.737$ ordered by increasing static energy, continued from fig. 40.

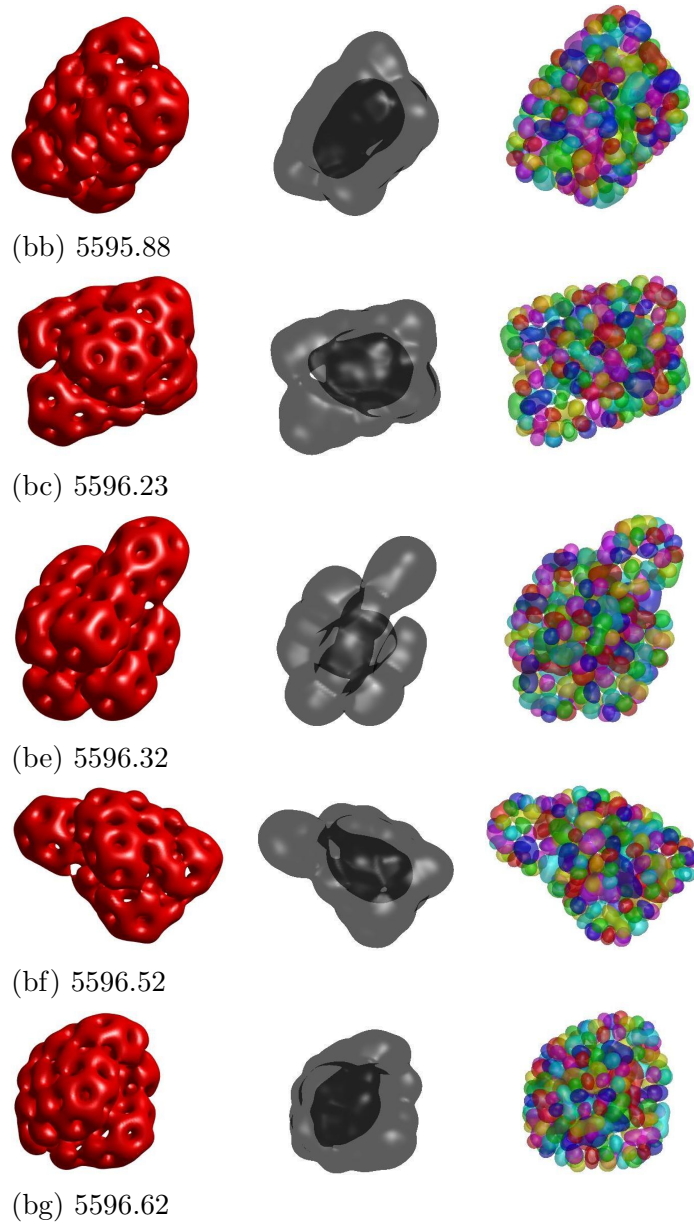


Figure 42: $B = 40$ solutions with $\kappa = 0.737$ ordered by increasing static energy, continued from fig. 41 and excluding those of figs. 23(left) and 26.

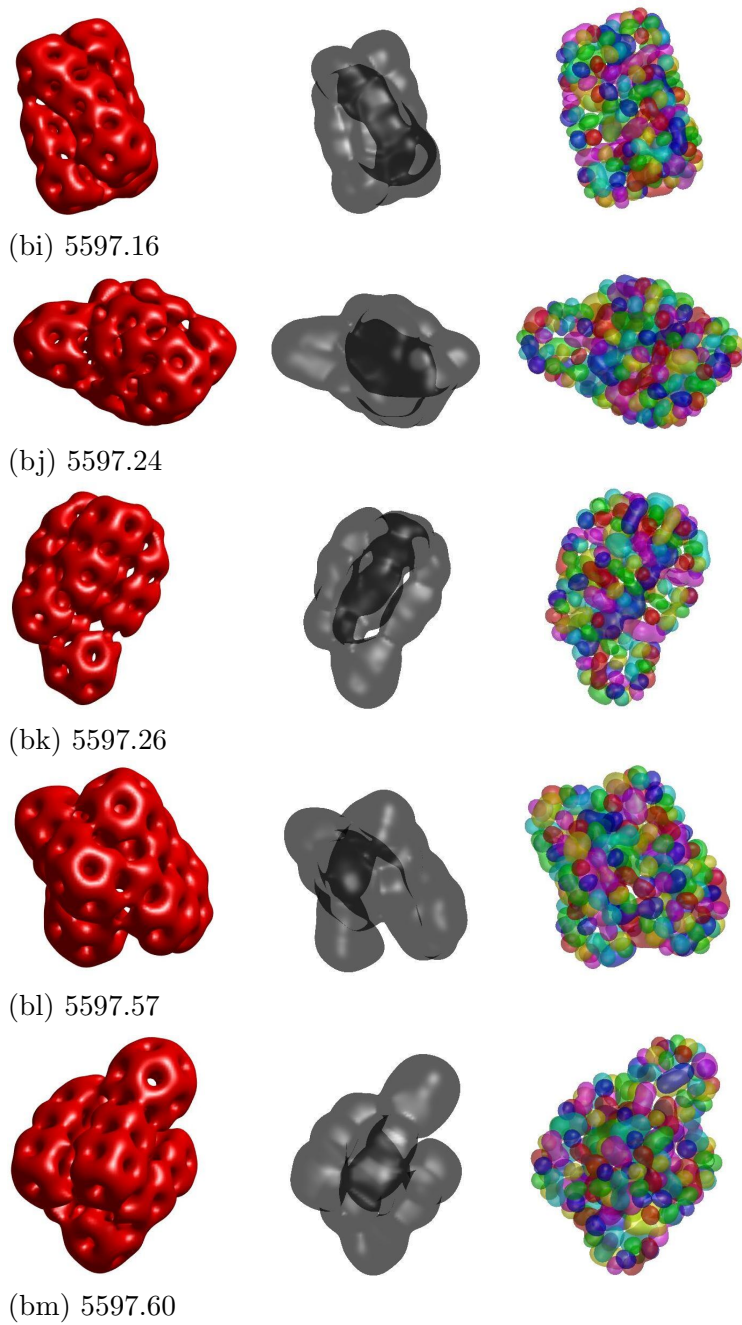


Figure 43: $B = 40$ solutions with $\kappa = 0.737$ ordered by increasing static energy, continued from fig. 42.

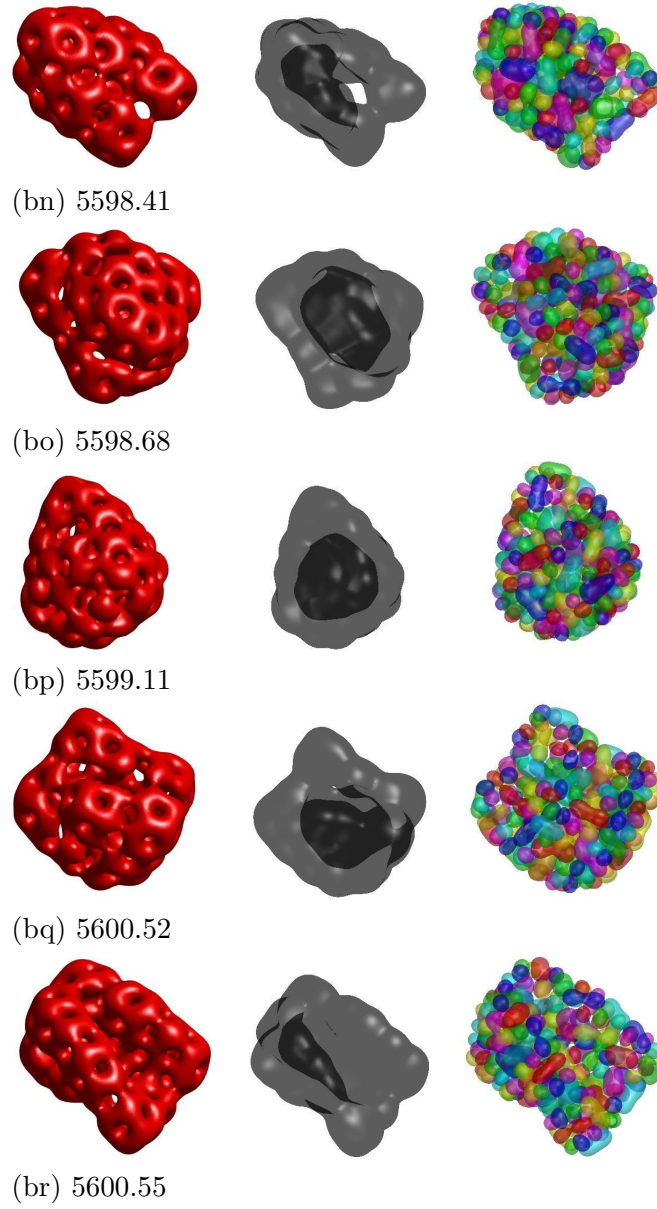


Figure 44: $B = 40$ solutions with $\kappa = 0.737$ ordered by increasing static energy, continued from fig. 43.

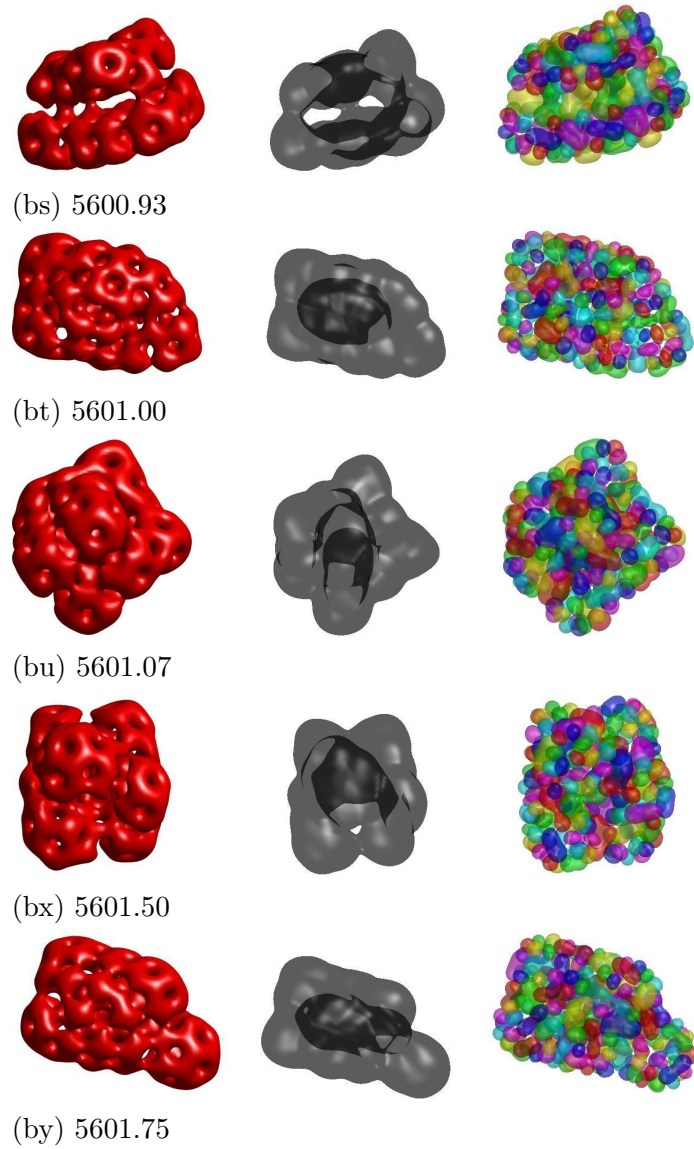


Figure 45: $B = 40$ solutions with $\kappa = 0.737$ ordered by increasing static energy, continued from fig. 44 and excluding that of fig. 24.

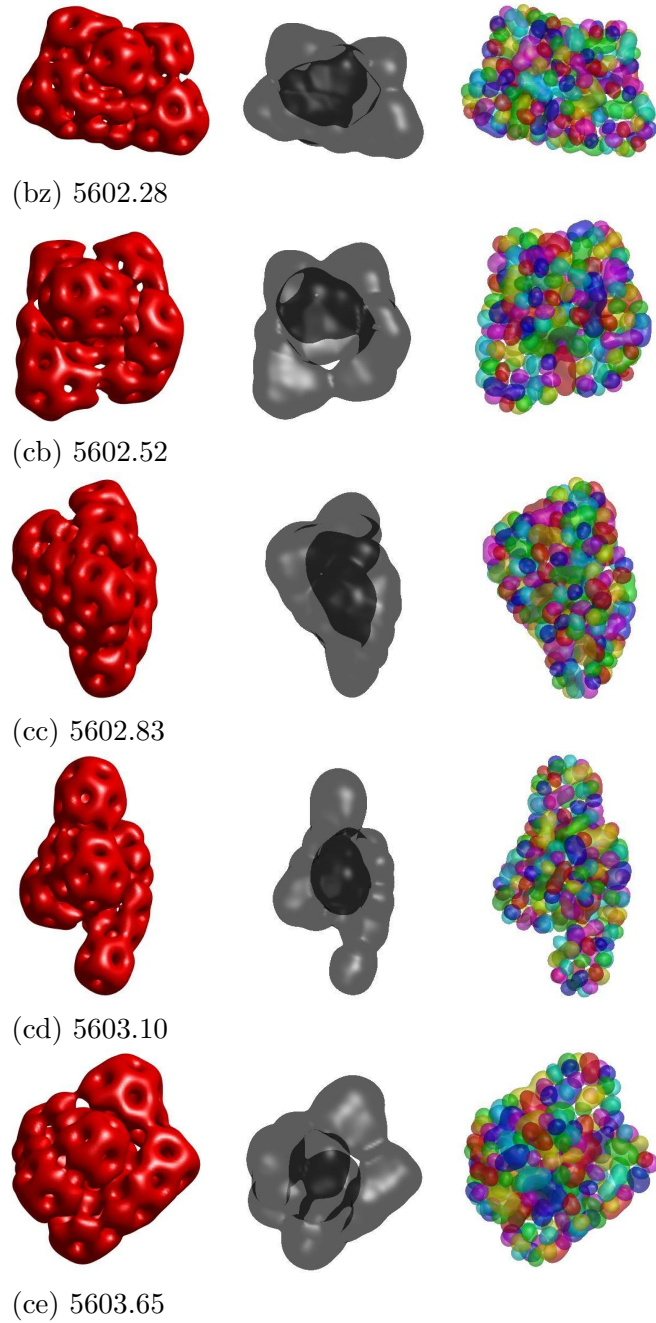


Figure 46: $B = 40$ solutions with $\kappa = 0.737$ ordered by increasing static energy, continued from fig. 45 and excluding that of fig. 23(right).

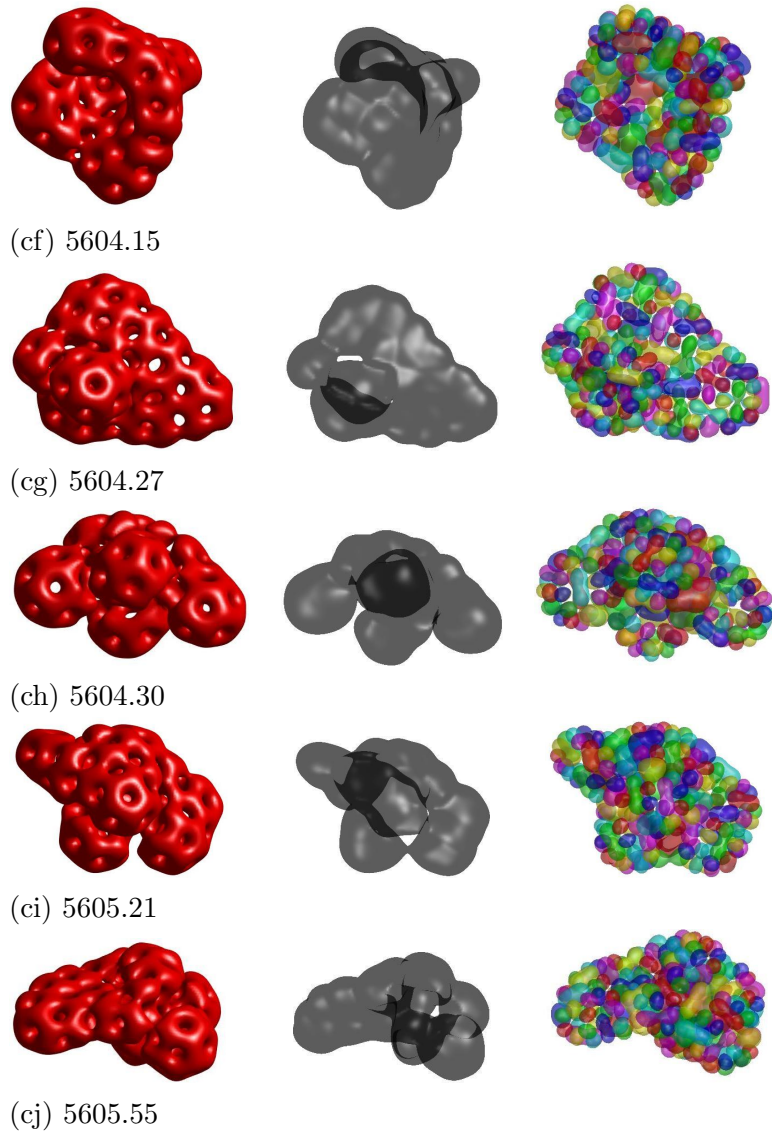


Figure 47: $B = 40$ solutions with $\kappa = 0.737$ ordered by increasing static energy, continued from fig. 46 and excluding the second last row of fig. 27.

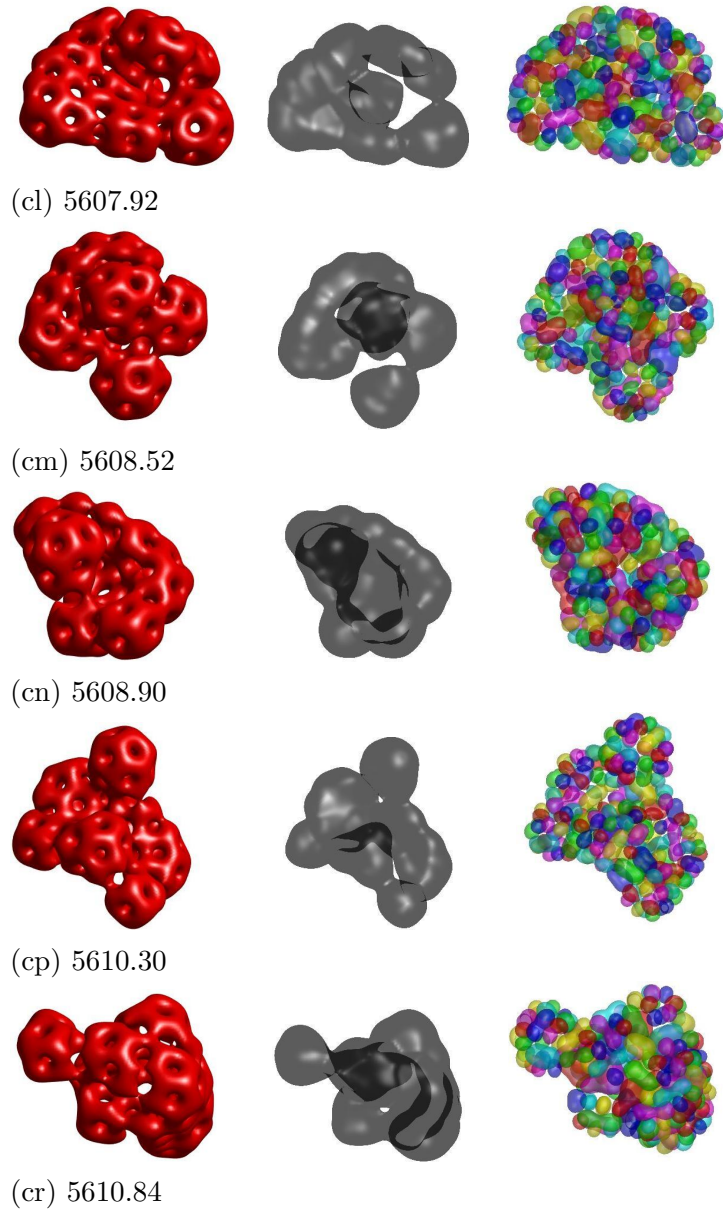


Figure 48: $B = 40$ solutions with $\kappa = 0.737$ ordered by increasing static energy, continued from fig. 47 and excluding the last row of fig. 27 as well as that of fig. 23(right).

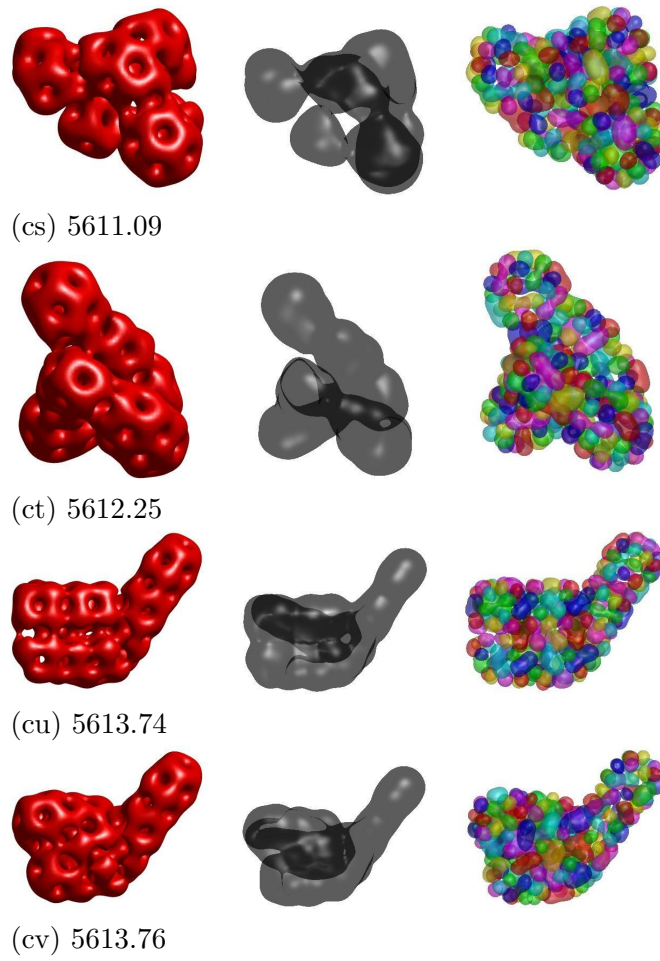


Figure 49: $B = 40$ solutions with $\kappa = 0.737$ ordered by increasing static energy, continued from fig. 48.